DUDLEY KNOX LIBRARY
NAVAL POSTGRADUATE SCHOOL
MONTEREY CA 93943-5101

Approved for public release; distribution is unlimited.

Numerical Analysis of Oscillating Flow About A Circular Cylinder

by

John E. Lotshaw
LCDR, United States Navy
B.S., University of Washington, Seattle, 1979

Submitted in partial fulfillment of the
requirements for the degree of

MASTER OF SCIENCE IN MECHANICAL ENGINEERING

from the

NAVAL POSTGRADUATE SCHOOL

June 1992

iclassified

:urity Classification of this page

REPORT DOCUMENTATION PAGE

Report Security Classification Unclassified	1b Restrictive Markings
Security Classification Authority	3 Distribution Availability of Report
Declassification/Downgrading Schedule	Approved for public release; distribution is unlimited.
Performing Organization Report Number(s)	5 Monitoring Organization Report Number(s)
Name of Performing Organization: ıval Postgraduate School	6b Office Symbol (*If Applicable*) 52
Address (*city, state, and ZIP code*): onterey, CA 93943-5000	7a Name of Monitoring Organization: Naval Postgraduate School
	7b Address (*city, state, and ZIP code*): Monterey, CA 93943-5000
Name of Funding/Sponsoring Organization	8b Office Symbol (*If Applicable*)
Address (*city, state, and ZIP code*)	9 Procurement Instrument Identification Number
	10 Source of Funding Numbers

Program Element Number	Project No	Task No	Work Unit Accession No

Title (*Include Security Classification*) Numerical Analysis of Oscillating Flow About A Circular Cylinder

Personal Author(s) John E. Lotshaw

a Type of Report	13b Time Covered	14 Date of Report (*year, month,day*)	15 Page Count
ıster's Thesis	From 01/92 To 06/92	June 1992	79

Supplementary Notation The views expressed in this thesis are those of the author and do not reflect the official ılicy or position of the Department of Defense or the U.S. Government.

Cosati Codes			18 Subject Terms (*continue on reverse if necessary and identify by block number*)
ld	Group	Subgroup	Numerical Calculations, Wake, Cylinder, Oscillating Flow, Wave and Current, Co-existing flow, Harmonically oscillating flow.

Abstract (*continue on reverse if necessary and identify by block number*

The numerical experiments, carried out through the use of the vorticity-stream function ıuations and their finite difference form, on sinusoidally-oscillating as well as co-existing flows inusoidal oscillation plus steady mean flow) at low and intermediate Keulegan-Carpenter ımbers are described. A third-order in time, second-order in space, three-level predictor-ırrector finite-difference scheme has been used. The Poisson equation for the stream function as solved by a Fast Poisson Solver based on the High Order Difference Approximation with .entity Expansion (HODIE) and the Fast Fourier Transform (FFT) methods provided by the ational Center for Atmospheric Research for the solution of separable elliptic partial fferential equations with a non-square grid. The analysis has produced force-transfer and fluid-ımping coefficients comparable to those obtained experimentally for both types of flows (i.e., ith and without current) and to those obtained with a square grid through the use of the IMSL ɔrary.

Distribution/Availability of Abstract	21 Abstract Security Classification
[X] unclassified/unlimited [ ] same as report [ ] DTIC users	Unclassified

a Name of Responsible Individual	22b Telephone (*Include Area code*)	22c Office Symbol
ofessor T. Sarpkaya (408) 646-3425	(408) 646-3425	ME-SL

) FORM 1473, 84 MAR 83 APR edition may be used until exhausted security classification of this page

All other editions are obsolete Unclassified

ABSTRACT

The numerical experiments, carried out through the use of the vorticity-stream function equations and their finite difference form, on sinusoidally-oscillating as well as co-existing flows (sinusoidal oscillation plus steady mean flow) at low and intermediate Keulegan-Carpenter numbers are described. A third-order in time, second-order in space, three-level predictor-corrector finite-difference scheme has been used. The Poisson equation for the stream function was solved by a Fast Poisson Solver based on the High Order Difference Approximation with Identity Expansion (HODIE) and the Fast Fourier Transform (FFT) methods provided by the National Center for Atmospheric Research for the solution of separable elliptic partial differential equations with a non-square grid. The analysis has produced force-transfer and fluid-damping coefficients comparable to those obtained experimentally for both types of flows (i.e., with and without current) and to those obtained with a square grid through the use of the IMSL library.

L82573
C.1

TABLE OF CONTENTS

DUDLEY KNOX LIBRARY
NAVAL POSTGRADUATE SCHOOL
MONTEREY CA 93943-5101

LIST OF TABLES

LIST OF FIGURES

NOMENCLATURE

A = amplitude of sinusoidal oscillations

a = transformation parameter

C_{IL} = inline force coefficient

C_L = transverse force coefficient

C_d^u = Fourier-averaged drag coefficient

C_m = inertia coefficient = $1 + k_{ij}^u$

D = diameter

F_{IL} = inline force

F_L = transverse force

K = Keulegan-Carpenter Number = $U_m T/D$

K^+ = K by current = $K(1 + U_o/U_m) = K + U_o T/D$

k_{ij}^u = Fourier-averaged added mass coefficient

n = order of polynomial (see Eq 17)

p_s = pressure on cylinder

p_∞ = pressure at outer boundary

$\bar{p}_s$ = pressure coefficient = $(p_s - p_\infty) / \rho U_\infty^2$

R = cylinder radius

Re = Reynolds number VU/ν, or $U_m D/\nu$

Re^+ = Re modified by current = $Re(1 + U_o/U_m) = Re + U_oD/\nu$

r = radial distance

T = period of oscillations

t = time

U = time dependent velocity

U_m = maximum velocity in pure sinusoidal flow

U_o = collinear steady current velocity

V = constant velocity reached at the end of the acceleration period

V_r = current ratio = U_o/U_m

β = $D^2/\nu T = Re/K$

$\Delta\alpha$ = disturbance oscillation applied to the ambient flow, (in degrees)

$\Delta\xi$ = computational grid spacing

Ω = relative displacement of fluid during the acceleration period

= $(S/R)_v = 0.5\ (dU/dt)\ t_v^2/R = 0.5\ V\ t_v/(R)$

μ = dynamic viscosity

ν = kinematic viscosity

ρ = density

θ = angular position

ψ = stream function

ω = vorticity

ACKNOWLEDGMENTS

For his support and guidance both as teacher and friend I express my sincere appreciation to Distinguished Professor T. Sarpkaya.

Many others have given me help along the way. Dave Marco and Tony Circelli have given me tremendous support using the ME and AERO computer labs. John Ekaterinares and Dr. Kwok of NASA provided the avenue for use of the CRAY supercomputers. LT K. Charles Vanover was instrumental in my introduction to the existing code. Professor Dalton and Dr. Xuegeng Wang supplied the initial program.

Finally my loving appreciation goes to my wife Jan for her continual support and understanding.

I. INTRODUCTION

Numerical experimentation in fluid dynamics, through the use of finite-difference, finite-element, and discrete-vortex methods, has attracted considerable attention during the past two decades and produced laminar flows difficult to measure and turbulent flows hard to verify and impossible to generalize. The reasons for this are relatively simple. Numerical solutions based on the full Navier-Stokes equations are not stable at high Reynolds numbers and the instability is non-linearly related to the particular flow, input parameters and the discretization conditions. Also, the real flow at the computed Reynolds numbers may be turbulent, at least in some regions of the flow, and the numerical experiment does not imitate the physical experiment. Furthermore, the observed physical and numerical instabilities do not necessarily correspond to each other. Assuming that the calculations for a given flow are carried out at sufficiently small Reynolds numbers, where the flow is known to remain stable and laminar, one quickly discovers that it is practically impossible to measure, to any credible degree of accuracy, most or all of the predicted quantities (except the Strouhal number and the photographs of the flow patterns).

Evidently, one's view of the state of the numerical modelling depends to a large extent on one's objectives. For example, if the objective is to obtain some approximate answers and flow kinematics, one might be perfectly satisfied with the existing codes. If the objective is to match the measured and calculated results (e.g., lift and drag coefficients), one might achieve the desired objective by fine tuning a number of model parameters (e.g., the order

of approximation of the velocity and/or vorticity gradients, particularly near the wall, mesh size, time step, type of discretization, outer boundary, just to name a few). If one's objectives are to perform numerical experiments for sake of numerical experiments, with no concern with the compatibility of the numerical and experimental results, then one can objectively asses the model instead of attempting to attribute to it artificial powers of prediction.

As far as the turbulent flows are concerned, some or all of the predictions of the numerical calculations for a given flow depend on the closure model used. Some models do better than others for some flows and worse than others for other flows. No model, however sophisticated, has a corner on the numerical market. Among the numerous theoretical, numerical, and experimental investigations, impulsively-started steady flow about a circular cylinder has occupied a prominent place partly because of its intrinsic interest towards the understanding of the evolution of separation, vortex formation, growth, and partly because it provided the most fundamental case for the comparison and validation of various numerical methods and codes. In recent years, attention has turned to a broader class of relatively manageable time-dependent flows about bluff bodies: Non-impulsively-started flows, sinusoidally oscillating flows, co-existing flows (uniform flow plus oscillating flow), flow from one steady state to another (at a lower or higher Reynolds number through the use of prescribed changes in velocity), and so on. The solution of these problems at sufficiently high Reynolds numbers will have far reaching theoretical and practical consequences. As noted above, this is not yet the case, and the solutions must necessarily be confined to cases where the accurate prediction of physical experiments and the instant gratification

are not the real objectives. However, it is hoped that even the approximate solutions will have enough information to elucidate the physics of the phenomenon.

The hydrodynamic loading situations which are well understood are those which do not involve flow separation. Thus, they are amenable to nearly exact analytical treatment. These concern primarily the determination of the fluid forces on large objects in the diffraction regime where the characteristic dimension of the body relative to the wave length is larger than about 0.2. The use of various numerical techniques is sufficient to predict accurately the forces and moments acting on the body, provided that the viscous effects and the effects of separation for bodies with sharp edges are ignored as secondary.

The understanding of the fluid-structure interactions which involve extensive flow separation and dependence on numerous parameters such as Reynolds number, Keulegan-Carpenter number, relative roughness, relative motion of the body, proximity effects, hydroelastic response, etc. is far from complete (Sarpkaya & Isaacson 1981). There are several reasons for this. First, although the physical laws governing the motion (the Navier-Stokes equations) are well understood, valid approximations necessary for numerical and physical model studies are still unknown. Even the unidirectional steady flow about a bluff body remains theoretically unresolved. Much of our understanding of vortex shedding behind bluff bodies came from steady-flow experiments, highly idealized models, and limited numerical solutions. Most of the numerical studies based on the use of the Navier-Stokes equations and some suitable spatial and temporal

differencing schemes are limited, out of necessity, to low Reynolds number flows. A second reason why progress has been slow is that the bluff body problems involving *wake return* are an order of magnitude more complex and there has been only a handful of limited applications of the methods based on Navier-Stokes equations.

The formation of a wake gives rise not only to a form drag, as it would be the case if the motion were steady, but also to significant changes in the inertial forces. The velocity-dependent form drag is not the same as that for the steady flow of a viscous fluid, and the acceleration-dependent inertial resistance is not the same as that for an unseparated unsteady flow of an inviscid fluid. In other words, the drag and inertial forces are interdependent as well as time-dependent. These effects are further compounded by the diffusion and decay of vortices and by the three-dimensional nature of vorticity due to turbulent mixing, finite spanwise coherence, and the random nature of the vortices (which give rise to cycle-to-cycle variations and numerous flow modes even under controlled laboratory conditions). The stronger and better correlated the returning vortices, the sharper and more pronounced the changes are in pressure distribution on the body and in the integrated quantities such as the lift, drag, and inertia coefficients.

It is clear from the foregoing that the objectives of the present investigation are to carry out extensive numerical experiments through the use of the vorticity-stream function form of the Navier-Stokes equations and their finite difference form, on co-existing flows (sinusoidal oscillation plus steady mean flow). The expectations are that the results will point out the strengths and weaknesses of the code, for the particular type of formulation

used, explain the reasons between the various numerical predictions of the same problem, and, hopefully, shed some light on the physics of flows heretofore uncalculated.

II. BACKGROUND STUDIES

A finite difference analysis of the Navier-Stokes equations for a sinusoidally-oscillating ambient flow about a circular cylinder at K (Keulegan-Carpenter Number) = U_mT/D = 5 (Re = 1000) and K = 7 (Re = 700) has been attempted by Baba & Miyata (1987). Their results have shown that the calculations can be carried out only for short times (less than two cycles of flow oscillation) with a non-super computer. Murashige, Hinatsu and Kinoshita (1989) have used a similar method to analyze three cases (K = 5, 7, and 10) at higher Reynolds numbers around 10^4. The flow was perturbed by artificial means to trigger an asymmetry. At K = 10, a transverse vortex street appeared, in agreement with experimental observations. The numerical simulation of steady flow past a circular cylinder undergoing in-line and/or transverse oscillations through the use of two-dimensional unsteady Navier-Stokes equations was undertaken by Lecointe et al. (1987) for relatively small amplitudes (A/D = 0.13). Justesen (1991) presented extensive results obtained from a numerical solution of a vorticity-stream function formulation of the Navier-Stokes equations for the flow around a circular cylinder in planar oscillating flow at small Keulegan-Carpenter numbers in the subcritical Reynolds number range. Justesen introduced a straining parameter "a" in order to better resolve the large gradients near the cylinder surface. This is in addition to the logarithmic straining, commonly used as part of the transformations, for a better resolution of the gradients near the body.

Evidently, Justesen's transformation for a = 0 defaults to the logarithmic straining. However, "a" becomes another disposable parameter, dependent on at least K and Re. Justesen had to choose judiciously the value of the straining parameter for each K in order achieve drag and inertia coefficients in satisfactory agreement with those obtained experimentally. A systematic numerical variation of the governing parameters for an arbitrary U(t) is extremely difficult.

The in-line oscillations of a cylinder in uniform flow (or the sinusoidally oscillating flow with a steady mean flow) has been the subject of intense interest in recent years (see, e.g., Sarpkaya & Isaacson, 1981 and Sarpkaya & Storm, 1985) in connection with the understanding of the behavior of hot-wire anemometers and the fluid loading of structures subjected to currents, gusts and other types of unsteady flows. The biassing of the shedding of the vortices by the current causes profound changes in both the drag and inertia coefficients, relative to their no-current values. The mobile separation points undergo large excursions, as much as 120 degrees during a given cycle of oscillation over a circular cylinder (Sarpkaya and Butterworth, 1992). These effects are further compounded by the diffusion and decay of vortices and by the three-dimensional nature of vorticity due to turbulent mixing, reduced spanwise coherence, mutual-induction instability, and the random nature of vortices which give rise to cycle-to-cycle variations and numerous flow modes even under controlled laboratory conditions. It is because of these reasons that the present work is dedicated to the numerical analysis of such flows.

III. NUMERICAL REPRESENTATION

A. COMPUTATIONAL METHOD

Here only a brief description of the computational method is presented. A more in depth description is given by Wang (1989) and Putzig (1991).

The fluid is assumed to be two-dimensional, incompressible and viscous. The governing equations for the solution are the Navier-Stokes equations, with the stream function and the vorticity as independent variables. To achieve a higher density of mesh points near the cylinder surface, the computational domain is transformed from the physical plane in Fig. 1 to a rectangular plane in Fig. 2 (see Appendix). In the rectangular plane, the mesh is maintained at a uniform grid spacing. It is necessary to have more mesh points closer to the cylinder surface because in this region the gradients of both the vorticity and the stream function are the largest.

A third-order in time, second-order in space, three-level predictor-corrector finite-difference scheme is used to solve the vorticity-transport equation. A Fast Poisson Solver automatically discretizes the separable elliptic equation which is then solved by a generalized cyclic reduction algorithm. One of the solvers was provided by the IMSL mathematics library, for the solution of separable elliptic partial differential equations with a *square* grid, and the other by the National Center for Atmospheric Research, for the solution of separable elliptic partial differential equations with a *non-square* grid.

The unsteady Navier-Stokes equations in the polar coordinates, as defined by the vorticity transport equation and the vorticity/stream-function equation are,

$$\frac{\partial \omega}{\partial t} - \frac{1}{r}\left[\frac{\partial}{\partial r}(\omega\frac{\partial \psi}{\partial \theta}) - \frac{\partial}{\partial \theta}(\omega\frac{\partial \psi}{\partial r})\right] = \nu\nabla^2\omega \tag{1}$$

and

$$\nabla^2\psi = \omega \tag{2}$$

where

$$\nabla^2 = \frac{\partial^2}{\partial r^2} + \frac{1}{r}\frac{\partial}{\partial r} + \frac{1}{r^2}\frac{\partial^2}{\partial \theta^2} \tag{3}$$

ω and ψ are the vorticity and the stream function, ν is the kinematic viscosity, t is the time and, r and θ are polar coordinates directions (see Fig. 1). The velocity components in the r and θ directions are defined by

$$u = -\frac{1}{r}\frac{\partial \psi}{\partial \theta} \quad \text{and} \quad v = \frac{\partial \psi}{\partial r} \tag{4}$$

The boundary conditions for the physical problem are:

(1) no slip and zero normal velocity on the surface of the cylinder

$$\psi = \frac{\partial \psi}{\partial r} = 0 \quad \text{on} \quad r = R \tag{5}$$

and (2) the potential flow at infinity is defined as

$$\psi = U(r - \frac{R}{r})\sin\theta \tag{6}$$

and $\omega = 0$ at $r = \infty$. U is the external flow and R is the radius of the cylinder.

The coordinate transformations required to go from the physical domain to the computational domain are:

$$r = R \exp(a\xi) \quad \text{and} \quad \theta = a\eta \tag{7}$$

where R is the radius of the cylinder and 'a' is a transformation parameter.

The transformation of the non-dimensionalized vorticity-stream function equations and their finite difference form through the use of the central difference approximation for vorticity and a two-step, three-level, predictor-corrector scheme, with a third order accuracy in time, are described in detail in Wang (1989), in Fredrickson (1990) and in Putzig (1991) and will not be repeated here.

B. CALCULATION OF THE FORCE COEFFICIENTS

The in-line and transverse force coefficients are determined from the combined contributions of the shear and pressure forces acting on the cylinder. The viscous forces are calculated from $\tau_s = \mu\omega$. The total in-line force then reduces to

$$F_{IL} = -\int_0^{2\pi} p_s \cos(\theta) R d\theta - \int_0^{2\pi} \mu\omega \sin(\omega) R d\theta \tag{8}$$

and the total lift force as

$$F_L = -\int_0^{2\pi} p_s \sin(\theta) R d\theta - \int_0^{2\pi} \mu\omega \cos(\omega) R d\theta \tag{9}$$

After dividing the in-line and the lift-force equations by $(0.5\ \rho U^2\ D)$ and defining

$$\overline{p}_s = \frac{2(p_s - p_\infty)}{\rho U_\infty^2} \tag{10}$$

the force coefficients reduce to

$$C_{IL} = -\frac{1}{2}\int_0^{2\pi} \overline{p}_s \cos(\theta) R d\theta - \frac{2}{Re}\int_0^{2\pi} \mu\overline{\omega} \sin(\omega) R d\theta \tag{11}$$

and

$$C_L = -\frac{1}{2}\int_0^{2\pi} \overline{p}_s \sin(\theta) R d\theta - \frac{2}{Re}\int_0^{2\pi} \mu\overline{\omega} \cos(\omega) R d\theta \tag{12}$$

The pressure coefficient is determined from the Navier-Stokes equations in terms of dimensionless vorticity. Once integrated with respect to θ, one has

$$\overline{p}_s(\theta) = \overline{p}_s(0) + \frac{4}{Re}\int_0^{2\pi}\left(\frac{\partial\overline{\omega}}{\partial\overline{r}}\right)_{r=1} d\theta \tag{13}$$

Equation (13) is substituted into equations (11) and (12) to determine the numerical scheme for the in-line and transverse force coefficients,

$$C_{IL} = -\frac{2}{Re}\int_0^{2\pi}\left\{\left[\int_0^{\theta}\left(\frac{\partial\overline{\omega}}{\partial\overline{r}}\right)_{r=1} d\theta\right]\cos(\theta) + \overline{\omega}\sin(\theta)\right\} d\theta \tag{14}$$

and

$$C_L = -\frac{2}{Re}\int_0^{2\pi}\left\{\left[\int_0^{\theta}\left(\frac{\partial\overline{\omega}}{\partial\overline{r}}\right)_{r=1} d\theta\right]\sin(\theta) + \overline{\omega}\cos(\theta)\right\} d\theta \tag{15}$$

The radial derivative of the vorticity on the surface of the cylinder, appearing in Equations (14) and (15), is determined through the use of discrete pointwise approximations of various orders, ranging from second to tenth order. For a second order approximation, one has

$$\left(\frac{\partial\overline{\omega}_i}{\partial\overline{r}}\right)_{r=1} = \frac{-3\omega_i + 4\omega_{i+1} - \omega_{i+2}}{2\Delta\xi} + O(\Delta\xi^2) \qquad (16)$$

For higher order polynomials Equation (16) may be written as

$$\left(\frac{\partial\overline{\omega}_i}{\partial\overline{r}}\right)_{r=1} = \frac{A\omega_i + B\omega_{i+1} + C\omega_{i+2} + D\omega_{i+3} + E\omega_{i+4} + \cdots\cdots}{\Delta\xi} + O(\Delta\xi^n) \qquad (17)$$

in which the coefficients A –K are given in Table 1 below.

Table 1: Coefficients of the Polynomial in Eq. (17)

	n=2	n=4	n=6	n=8	n=10
A	-3/2	-25/12	-49/20	-761/280	-7381/2520
B	2	4	6	8	10
C	-1/2	-3	-15/2	-14	-45/2
D		4/3	20/3	56/3	40
E		-1/4	-15/4	-35/2	-105/2
F			6/5	56/5	252/5
G			-1/6	-14/3	-35
H				8/7	120/7
I				-1/8	-45/8
J					10/9
K					-1/10

C. CALCULATION OF THE DRAG AND INERTIA COEFFICIENTS

If one were to associate the total force with a velocity-square-dependent drag force and an acceleration-dependent inertial force then the coefficient associated with the latter may be interpreted as some measure of the added mass. But one must bare in mind that such a decomposition is far from being unique.

It has been customary to express the fluid force acting on a body moving in a fluid otherwise at rest as

$$F(t) = \frac{1}{2}\rho C_d^u A_p \left|\{(U_o + U(t)\}\right| \{(U_o + U(t)\} + \rho k_{ij}^u \forall \frac{dU(t)}{dt} \tag{18}$$

where U_o represents the steady velocity; U(t), the time-dependent oscillations; C_d^u , the Fourier-averaged drag coefficient and k_{ij}^u , the Fourier-averaged added-mass coefficient. It is customary to use an inertia coefficient C_m for a fluid in motion about a body at rest through the use of $C_m = 1 + k_{ij}^u$.

The Fourier averages of the drag and added-mass coefficients over a period of T may be calculated by multiplying both sides of Equation (8) once with **U(t)** and once with **dU/dt** to yield

$$C_d^u = \frac{2\int_0^T F(t)U(t)dt}{\rho A_p \int_0^T \left|\{(U_o + U(t)\}\right| \{(U_o + U(t)\} U(t)dt} \tag{19}$$

and

$$(Cm - 1) = k_{11}^{u} = \frac{\int_0^T F(t)\frac{dU(t)}{dt}dt}{\rho\forall\int_0^T [dU(t)/dt]^2 dt} \tag{20}$$

which may be evaluated readily provided that sufficiently reliable data are available for F(t), U_o, U(t), and dU(t)/dt.

A simple dimensional analysis of the flow under consideration shows that the time-averaged force coefficients (C_d^u and k_{ij}^u) are functions of a relative amplitude or Keulegan-Carpenter number, Mach number, Reynolds number, and a parameter involving U_o (e.g., U_oT/D or $U_o/[U(t)]_{max}$). There are numerous possibilities regarding the definitions of the relative amplitude or Keulegan-Carpenter number and the Reynolds number. The purpose of the search for a more suitable Keulegan-Carpenter number and/or Reynolds number is to enhance the correlation of the data to reduce the number of the governing parameters, possibly eliminating U_oT/D as an independent parameter. The list of possible Reynolds numbers and Keulegan-Carpenter numbers is long and will not be given here. Suffice it to note that the two force-coefficients for the flow about a cylinder may be written as

$$\begin{matrix} C_d^u \\ k_{ij}^u \end{matrix} = f_i(K, Re, VK) \tag{21}$$

or as

$$\frac{C_d^u}{k_{ij}^u} = f_i(K^+, Re^+, VK) \tag{22}$$

in which

$$K = U_m T/D \quad , \quad Re = U_m D/\nu \quad , \quad VK = U_0 T/D$$

$$K^+ = K(1 + U_0/U_m) = K + U_0 T/D$$

$$Re^+ = Re(1 + U_0/U_m) = Re + U_0 D/\nu \tag{23}$$

The purpose of the present calculations was not to provide a detailed comparison between the measured and calculated forces but rather to attempt to establish a relationship between the shedding of vortices and the relative magnitude of the current. The particular values of K and V_r chosen for the calculations (K = 4 – 6, V_r = 0.0 – 1.2) was one for which some experimental data were available at comparable β, Re, and V_r values.

IV. DISCUSSION OF RESULTS

The numerical experiments were carried out through the use of a VAX-2000, a VAX-3520, a CRAY Supercomputer. The solution procedure and technique have been validated for several types of unsteady flows, i.e., impulsively-started, suddenly-stopped, and uniformly-decelerated flows before applying it to co-existing flows (oscillatory flow or sinusoidally-oscillating flow with mean velocity). Excellent agreement with flow visualization and experimentally determined drag and lift coefficients has been obtained for both symmetric and asymmetric wake solutions. It is this validation that led to the exploration of the characteristics of sinusoidally-oscillating flows superimposed on a mean velocity. The oscillation was specified by $U = U_o + U_m \sin(2\pi t/T)$ in which U_o is the steady mean velocity and U_m is the amplitude of sinusoidal oscillations.

The flow was perturbed by changing the direction of the ambient flow sinusoidally (with an amplitude of one-half of a degree) during the first cycle of the oscillation. The amplitude of the sine wave was the only free parameter. It is worth noting that this type of disturbance gradually returns the perturbed quantity to its initial state.

Numerical experiments have been carried out in the range of K = 1–4, β = 200, Re = 200–800, Δt = 0.00025–0.0005 and for various values of $V_r = U_o/U_m$, as shown in Table 2.

Table 2 The range of the governing parameters
($\beta = 200$)

V_r / K =	1	2	3	4
0.0	X	X	X	X
0.60				X
0.65				X
0.70				X

Evidently, this is a rather limited exploration of a highly complex problem and requires much more numerical and experimental work. The purpose of the present calculations was not to provide a detailed comparison between the measured and calculated forces but rather to attempt to establish a relationship between the shedding of vortices and the relative magnitude of the current.

Figures 3 through 6 show for K = 1, $\beta = 200$, $V_r = 0.0$, and $\Delta t = 0.00025$, the in-line force and streamlines. The calculated force coefficients are $C_d = 2.18$ and $C_m = 2.15$. The corresponding theoretical values are $C_d = 2.2$ and $C_m = 2.1$ (Wang 1968). Figures 7–13 show the in-line force, the streamlines and the streaklines, for K = 2, $\beta = 200$, and $V_r = 0.0$. The calculated force coefficients are $C_d = 1.35$ and $C_m = 2.13$. The corresponding theoretical and experimental values are, respectively, C_d (th) = 0.95, C_d (exp) = 1.50 and C_m (th) = 2.02 and C_m (exp) = 2.0. The differences between the calculated, experimental, and theoretical values are due to the fact that the theoretical values do not account for the flow separation. Figures 14–24 show the in-line force and

detailed streakline plots for K = 3, β = 200, and V_r = 0.0. The calculated force coefficients are C_d = 1.35 and C_m = 2.02. The corresponding experimental values (Bearman et al. 1985) are C_d = 1.45 and C_m = 2.10. There are no theoretical values to compare with for the reasons just cited. Figures 25–31 show the in-line force and the streaklines for K = 4, β = 200, and V_r = 0.0. The calculated force coefficients are C_d = 1.38 and C_m = 1.92. The corresponding experimental values (Bearman et al. 1985) are C_d = 1.45 and C_m = 1.95. It is clear from the foregoing that for the no-current case the calculated force-transfer coefficients are in very good agreement with those obtained experimentally. For the cases for which a comparison is possible, the calculated values also agree reasonably well with the theoretical values of Wang (1968).

Figures 32–38 show the in-line and transverse forces, the streamlines and the streaklines for K = 4 and V_r = 0.6 (with C_d= 1.17, C_m = 1.65); and Figs. 39–41 show the in-line and transverse forces and a single streakline plot for K = 4 and V_r = 0.65 (with C_d= 1.16, C_m = 1.63); and finally, Figs. 42-43 show a streamline and a streakline plot for K = 4 and V_r = 0.7 (with C_d= 1.15, C_m = 1.63).

The calculation with current were carried out for the expressed purpose of substantiating the previous findings that for K = 4, within a narrow range of V_r values, the width of the wake increases and the vortices begin to arrange themselves along three rows. In order to make sure that this finding was not a consequence of the sensitivity of the code to grid shape and size and the time-interval used, a more comprehensive series of calculations were

undertaken through the use of a non-square grid. Not only were the previous conclusions substantiated but also additional facts were uncovered. A comparison of Fig. 38 (for $V_r = 0.60$), with Fig. 41 (for $V_r = 0.65$), and Fig. 43 (for $V_r = 0.7$) shows that the wake is comprised of three rows of heterostrophic vortices. They differ only in detail from one V_r to another in the narrow range of V_r values from about 0.6 to 0.7. At lower V_r values, the inner pair of vortices are closer to the wake axis. As V_r increases toward 0.7, the inner pair reaches the edges of the outer pair (Fig. 43), and the inner and the outer vortices form an interesting quadruple. The vortex pairs on one side of the street may propel themselves (as a Kelvin oval) away from the wake axis, or become part of a larger scale instability. In either case, it will be difficult to predict the behavior of such a special wake at larger times because it is rather difficult to distinguish between the naturally occurring instabilities and those occurring numerically due to truncation errors. Nevertheless, it is gratifying to note that the flow visualization of the early stages of the wake for $K = 4$, at a representative value of $V_r = 0.65$, yielded results in excellent agreement with those presented herein.

Table 3 shows a comparison of the calculated and experimental (Moe & Verley 1980) drag and inertia coefficients for $K = 4$ for representative values of V_r. As expected, the inertia coefficients agree extremely well. As far as the drag coefficients are concerned, the agreement is not as good but certainly better than expected in view of the fact that β was 200 in the calculations and about 600 in the experiments. Nevertheless, the trend of the data is well predicted.

Table 3. Comparison of the Measured and Calculated Force Coefficients for K = 4 and Three Values of V_r

V_r:	0.60	0.65	0.70
C_m^u (exp)	1.68	1.63	1.60
C_m^u (cal)	**1.65**	**1.63**	**1.63**
C_d^u (exp)	0.93	0.98	1.05
C_d^u (cal)	**1.17**	**1.16**	**1.15**

V. CONCLUSIONS

The investigation reported here warranted the following conclusions:

1. Even the higher order finite difference formulations of the governing equations based on the vorticity/stream-function formulation of the Navier Stokes equations can be solved for only relatively small Reynolds numbers. This is primarily due to stability and computer constraints.

2. The numerical experiments with pulsating flows (oscillation plus steady mean flow) for K = 4 yielded force-transfer coefficients in good agreement with those obtained experimentally.

3. For K = 4 and relative current velocities of about 0.6–0.7, the vortices shed nearly symmetrically at each cycle and gave rise to a most unusual three-row vortex street, where each row is comprised of a pair of heterostrophic vortices. For relative current velocities larger than about one, the vortex wake returned to the asymmetric mode, as is encountered in a regular Karman vortex street. The use of a non-square grid in lieu of a square grid in solving the Poisson's equation did not alter the results.

4. The foregoing numerical experiments could not have been possible had it not been due to the availability of a VAX-3520 and a CRAY supercomputer. It is fully realized that numerical instabilities versus fluid dynamical instabilities have different and at times competing mathematical and computational demands. It is because of this reason that calculations at higher Reynolds numbers (while preserving flow stability) and calculations at very small Keulegan-Carpenter numbers (while preserving numerical stability) require extremely large CPU times even on a supercomputer.

APPENDIX

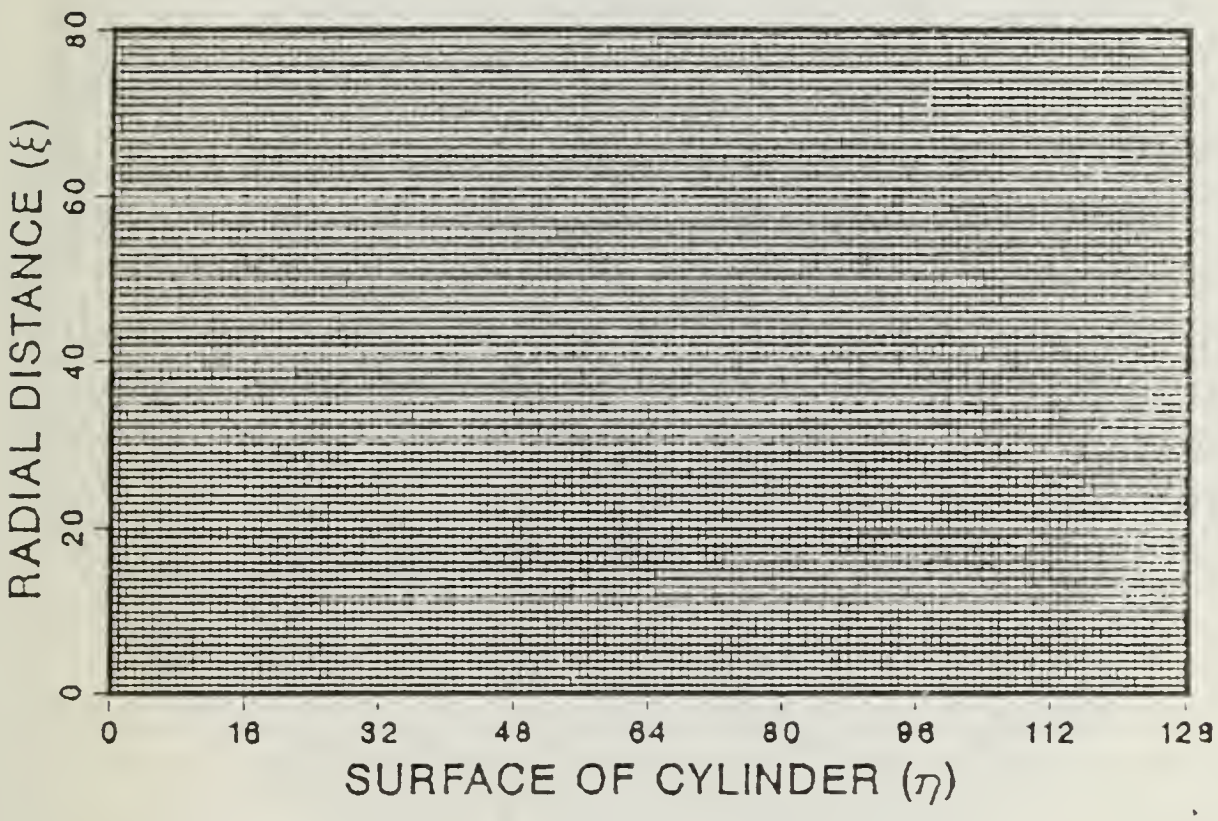

Figure 1. Grid in the Computational Domain

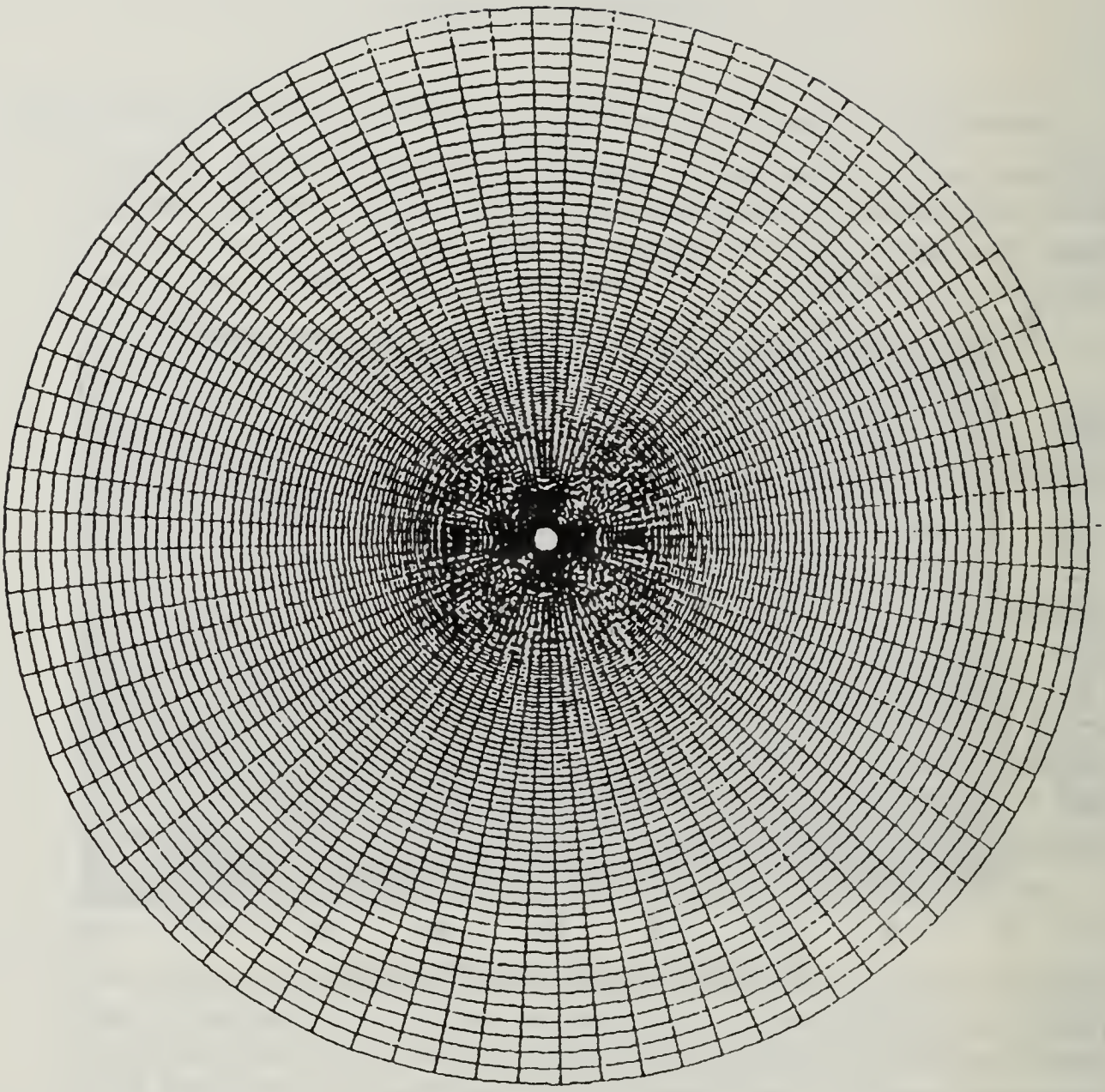

Figure 2. Grid in the Physical Domain

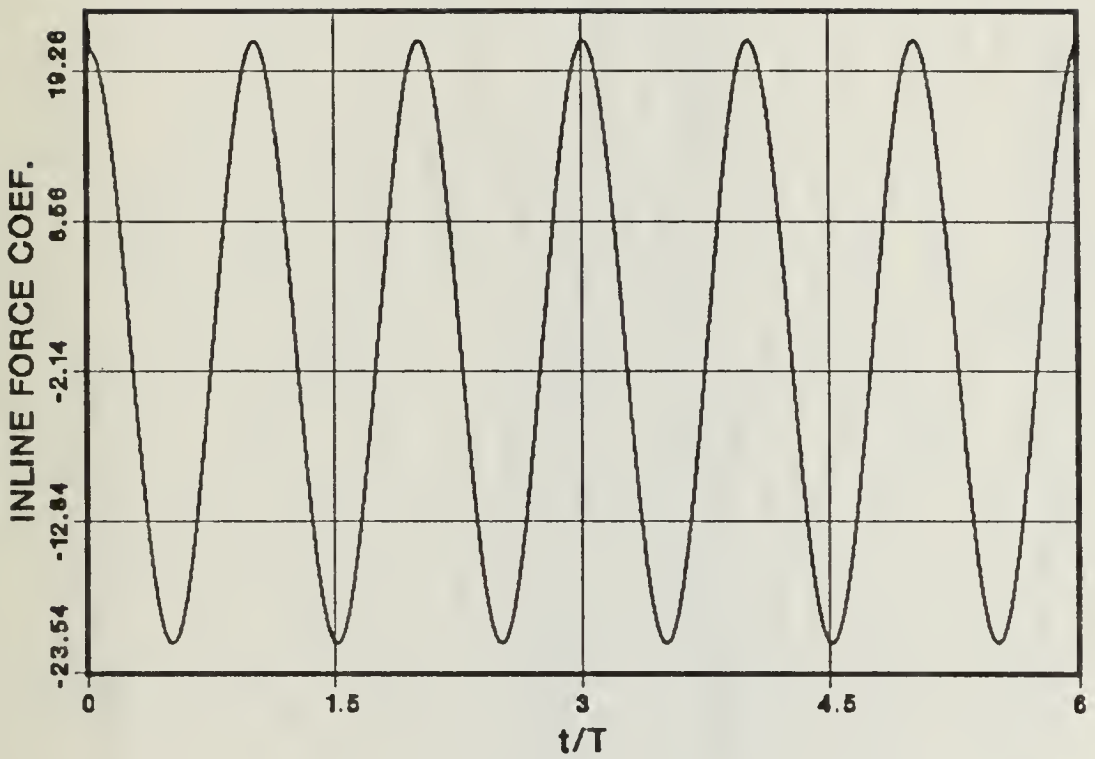

Figure 3. In-Line Force Coefficient, K = 1, Re = 200, V_r = 0.0

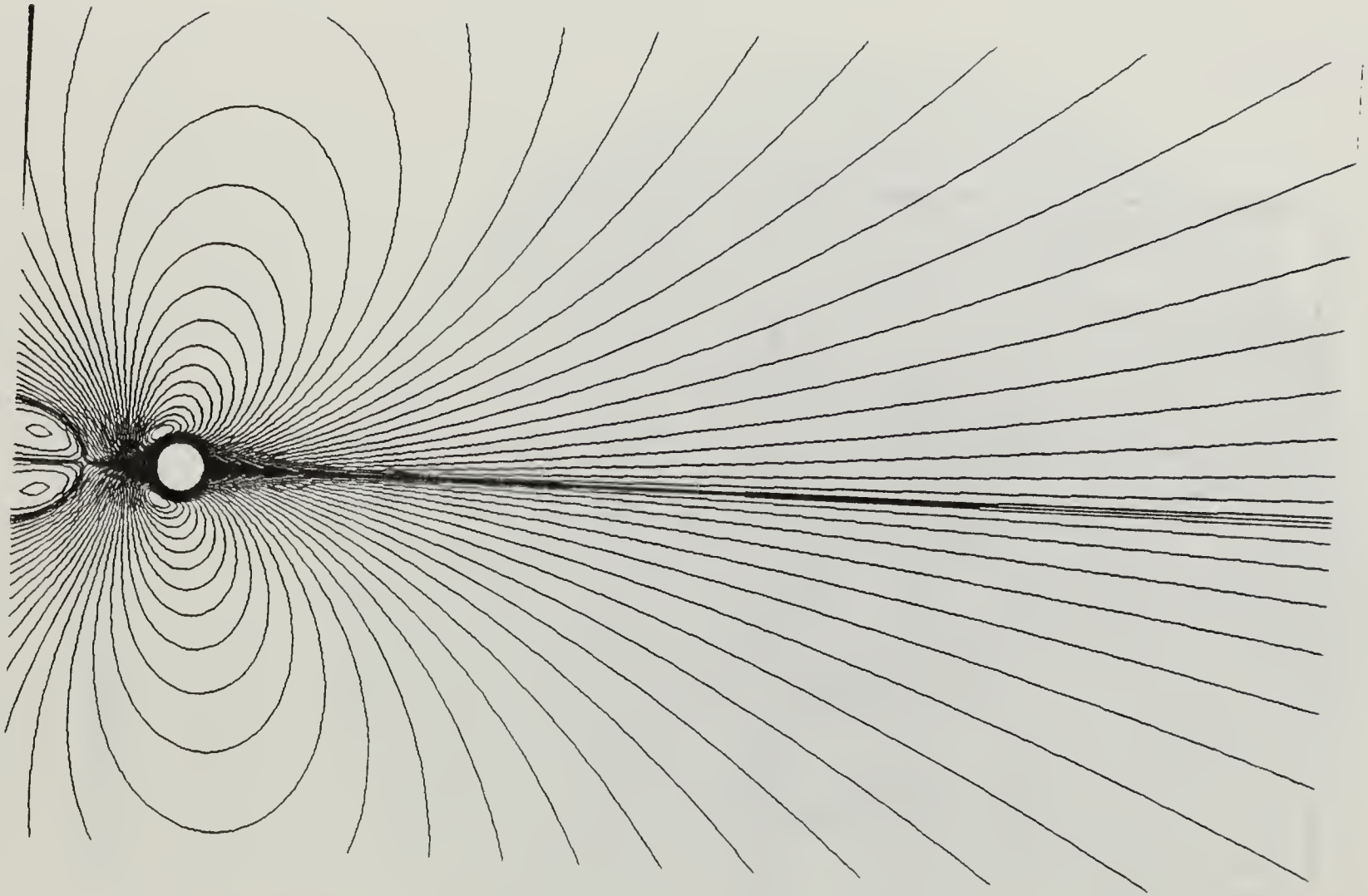

Figure 4. Streamlines, K = 1, Re = 200, V_r = 0.0, t/T = 4.0

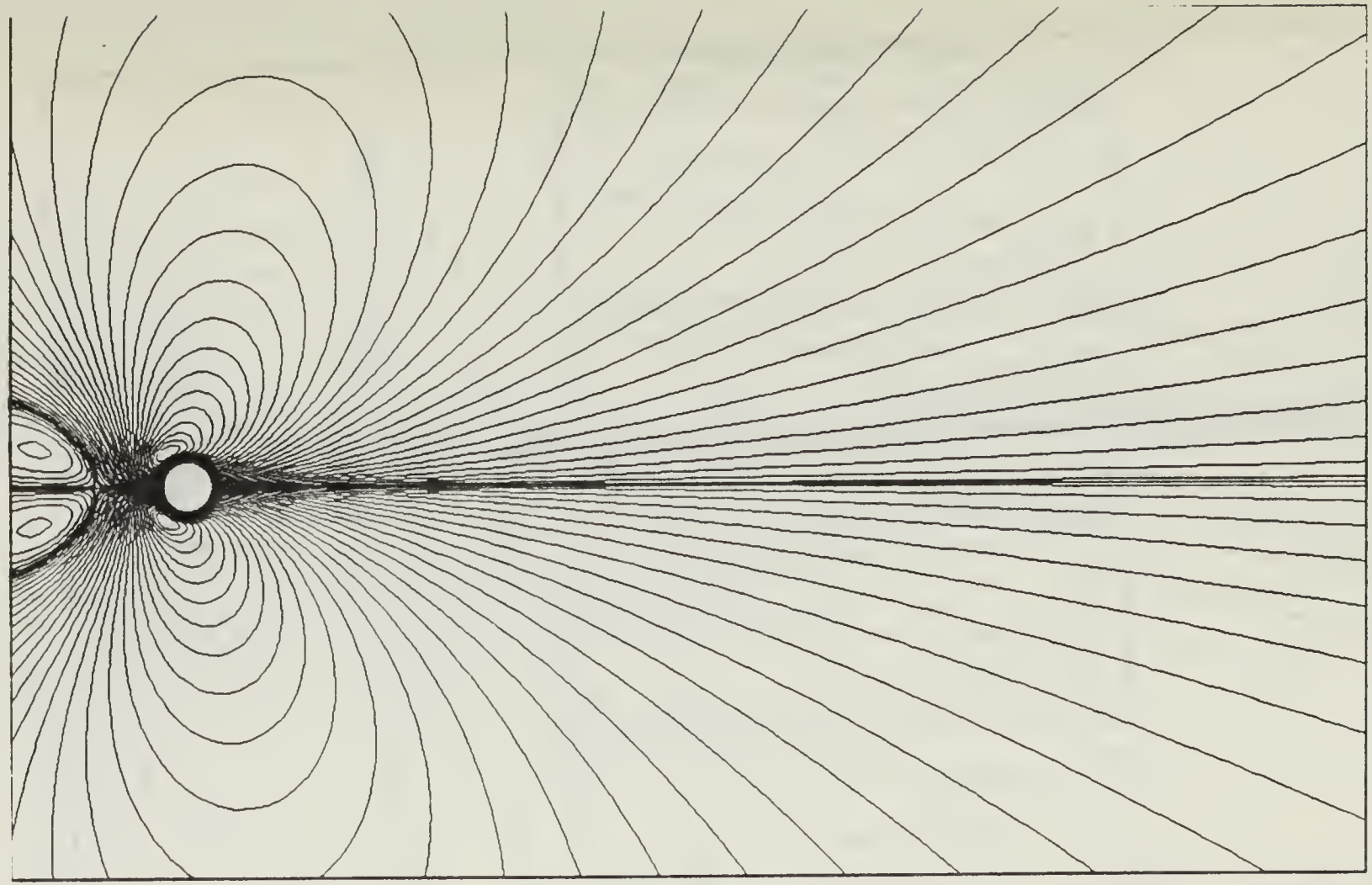

Figure 5. Streamlines, K = 1, Re = 200, V_r = 0.0, t/T = 5.0

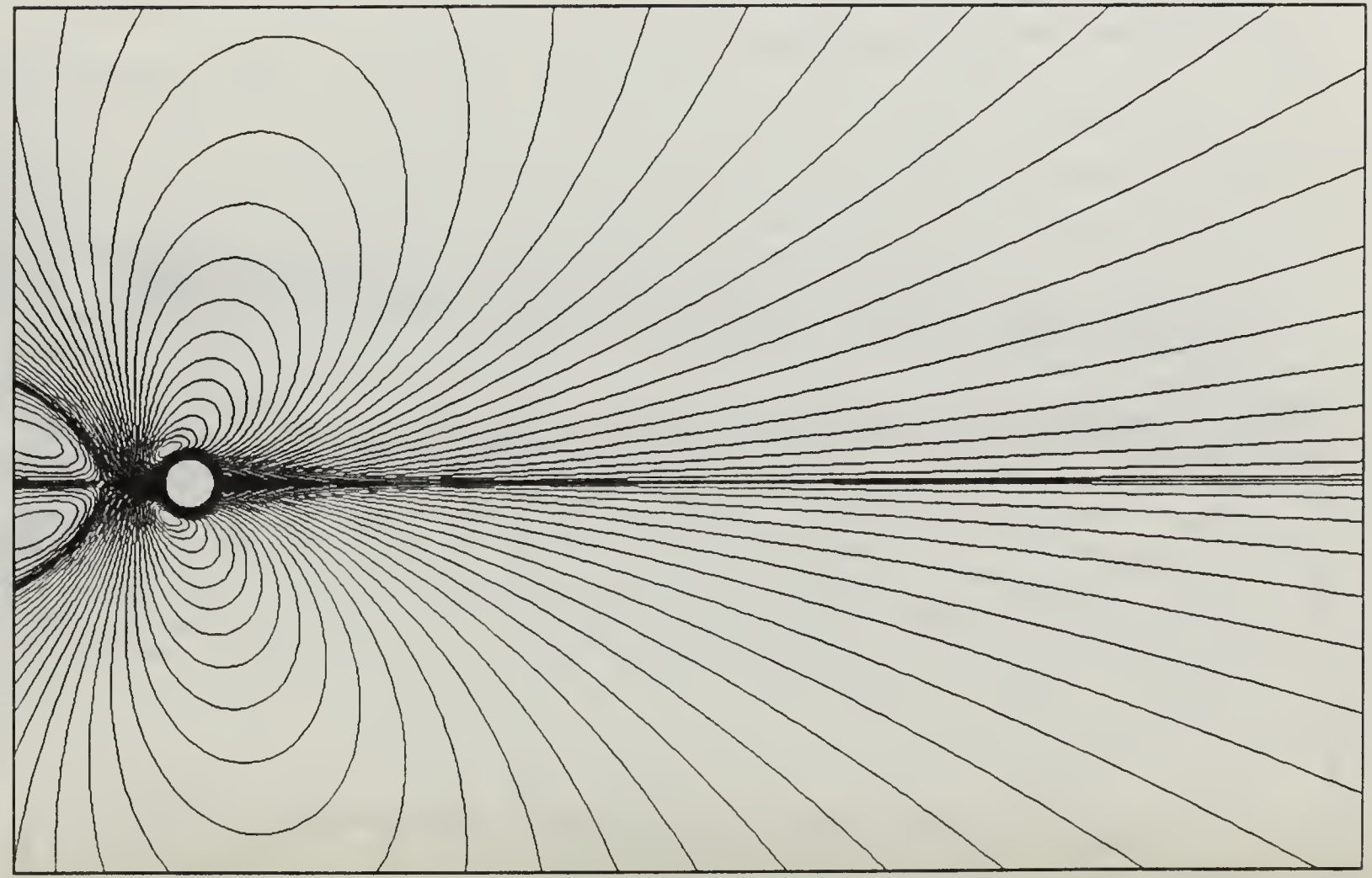

Figure 6. Streamlines, K = 1, Re = 200, V_r = 0.0, t/T = 6.0

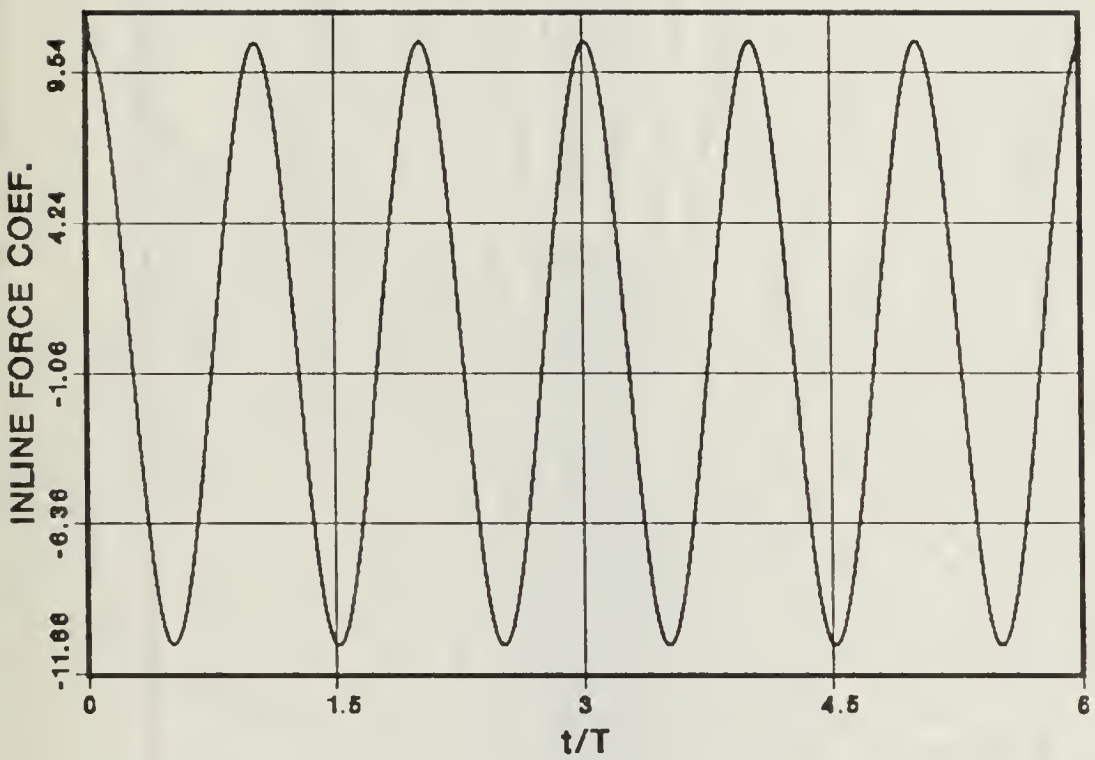

Figure 7. In-Line Force Coefficient, K = 2, Re =400, V_r = 0.0

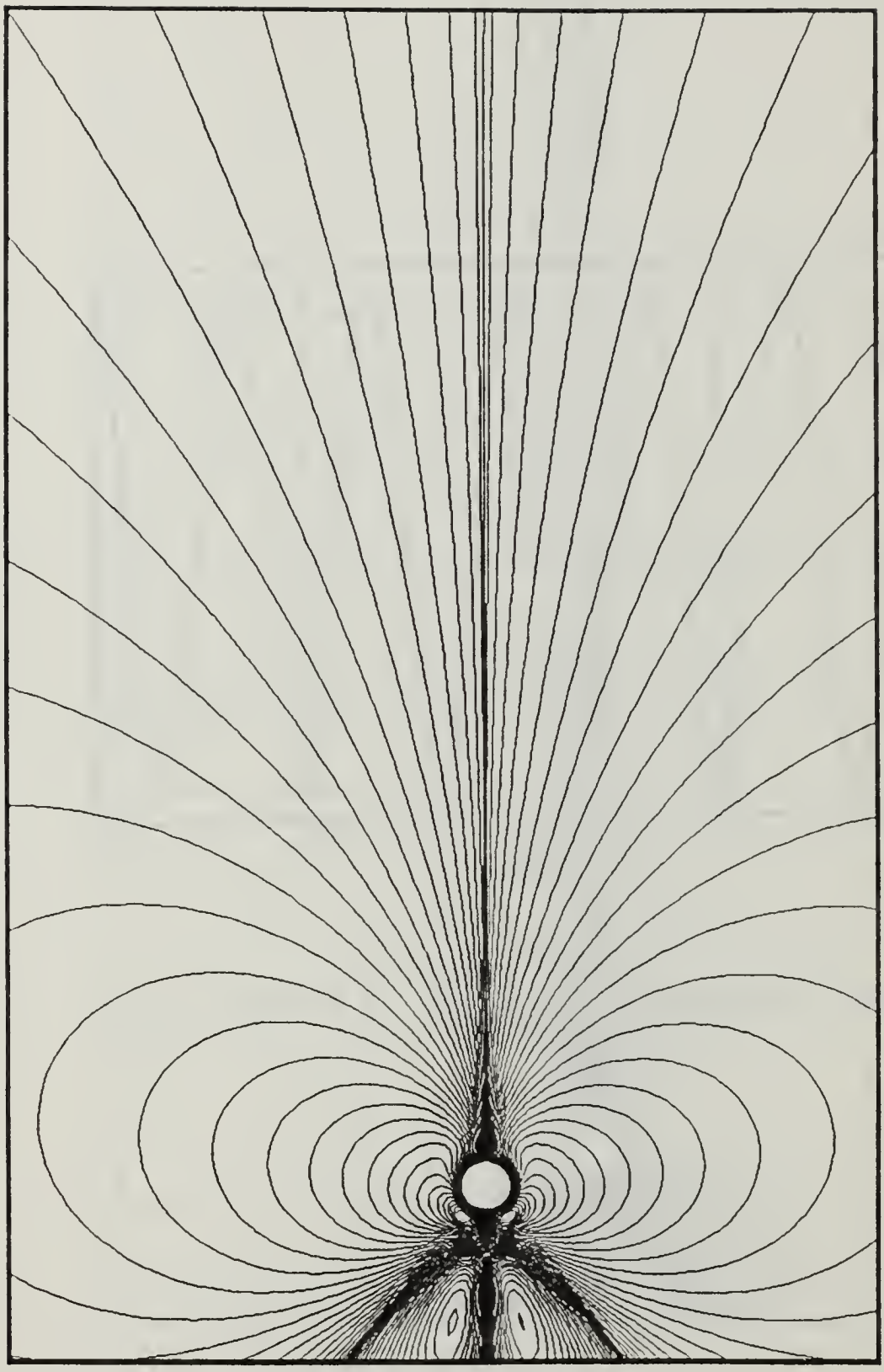

Figure 8. Streamlines, K = 2, Re =400, V_r = 0.0, t/T = 4.0

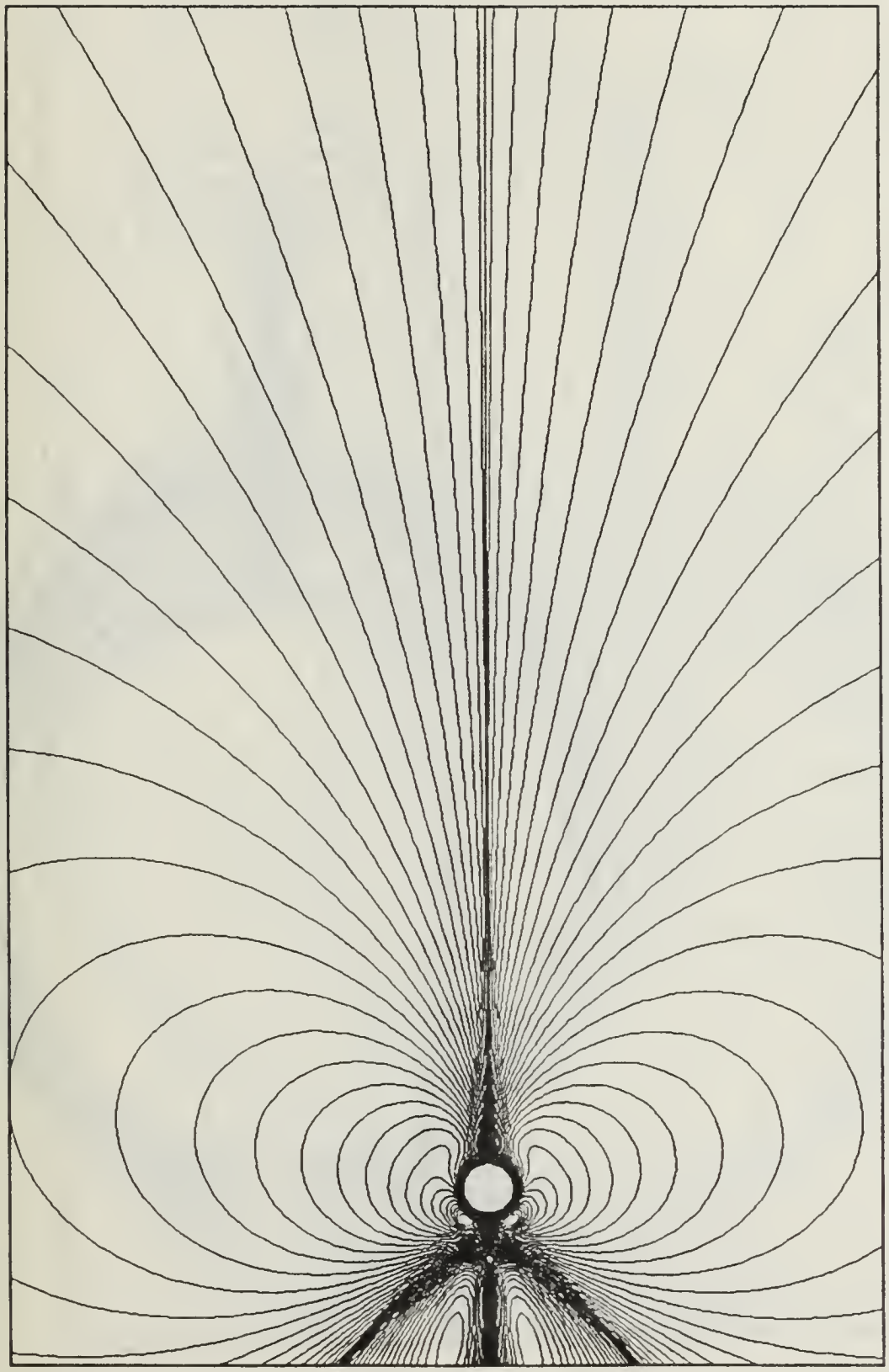

Figure 9. Streamlines, K = 2, Re =400, V_r = 0.0, t/T = 5.0

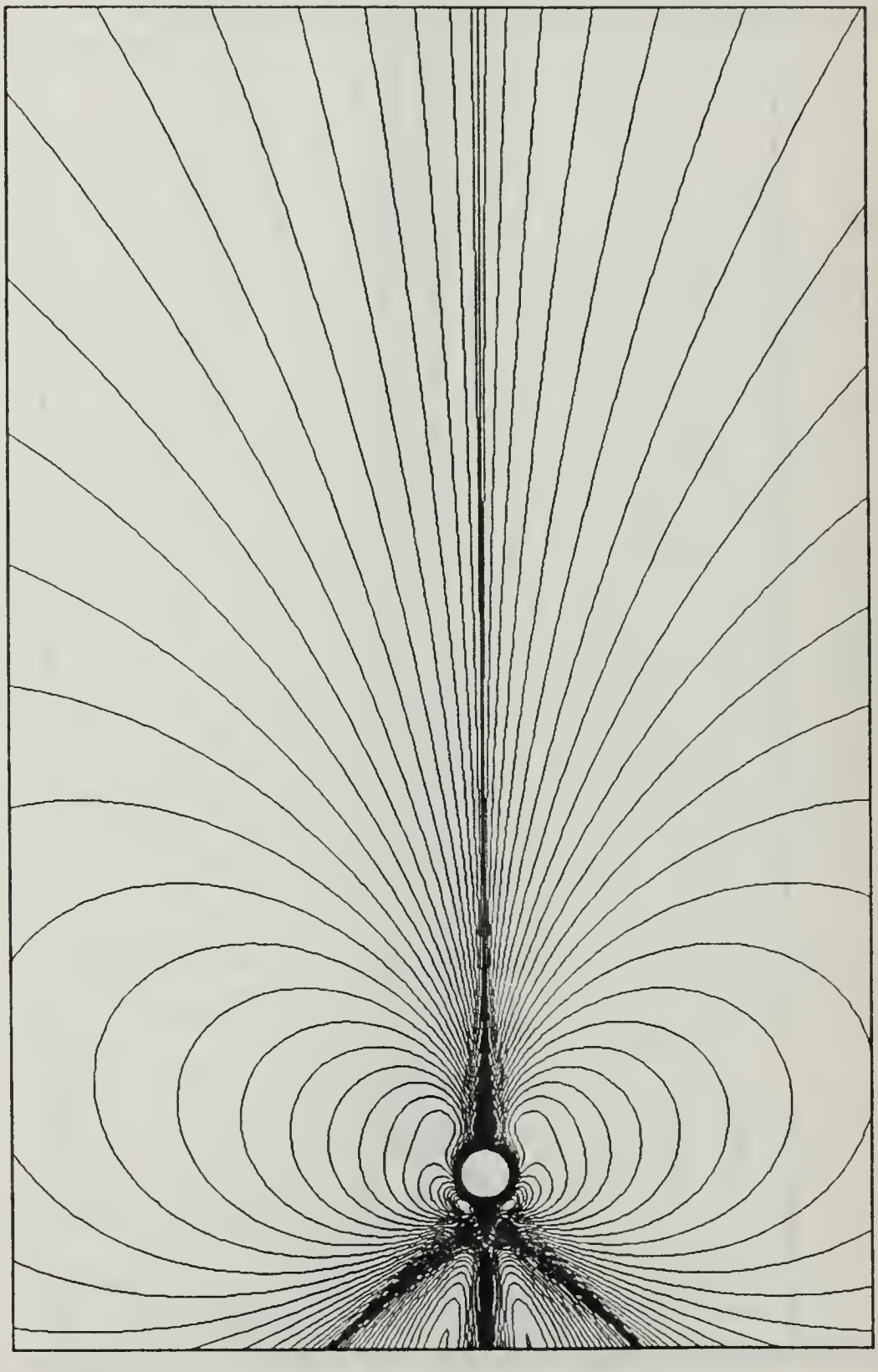

Figure 10. Streamlines, K = 2, Re =400, V_r = 0.0, t/T = 6.0

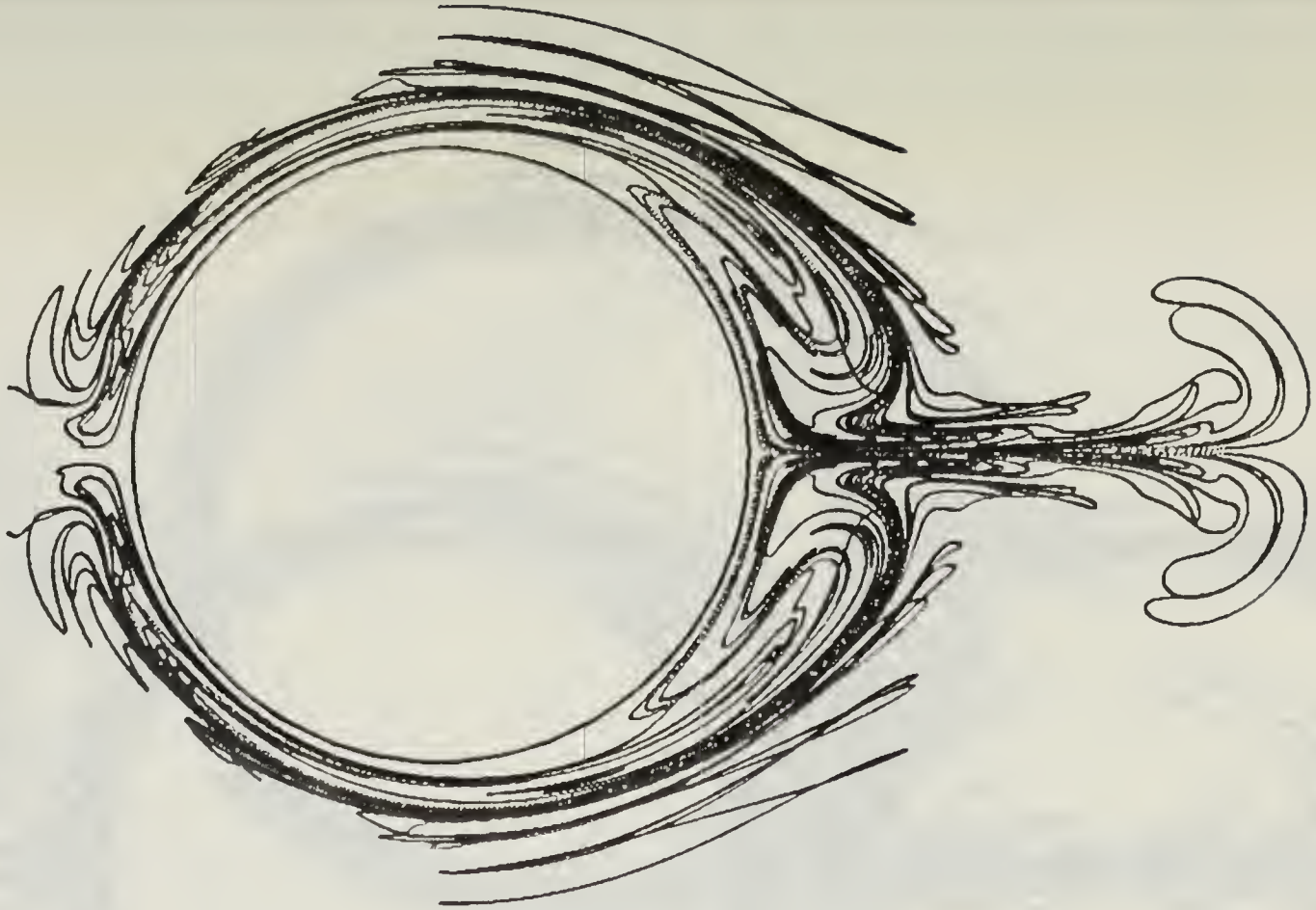

Figure 11. Streaklines, K = 2, Re =400, V_r = 0.0, t/T = 4.0

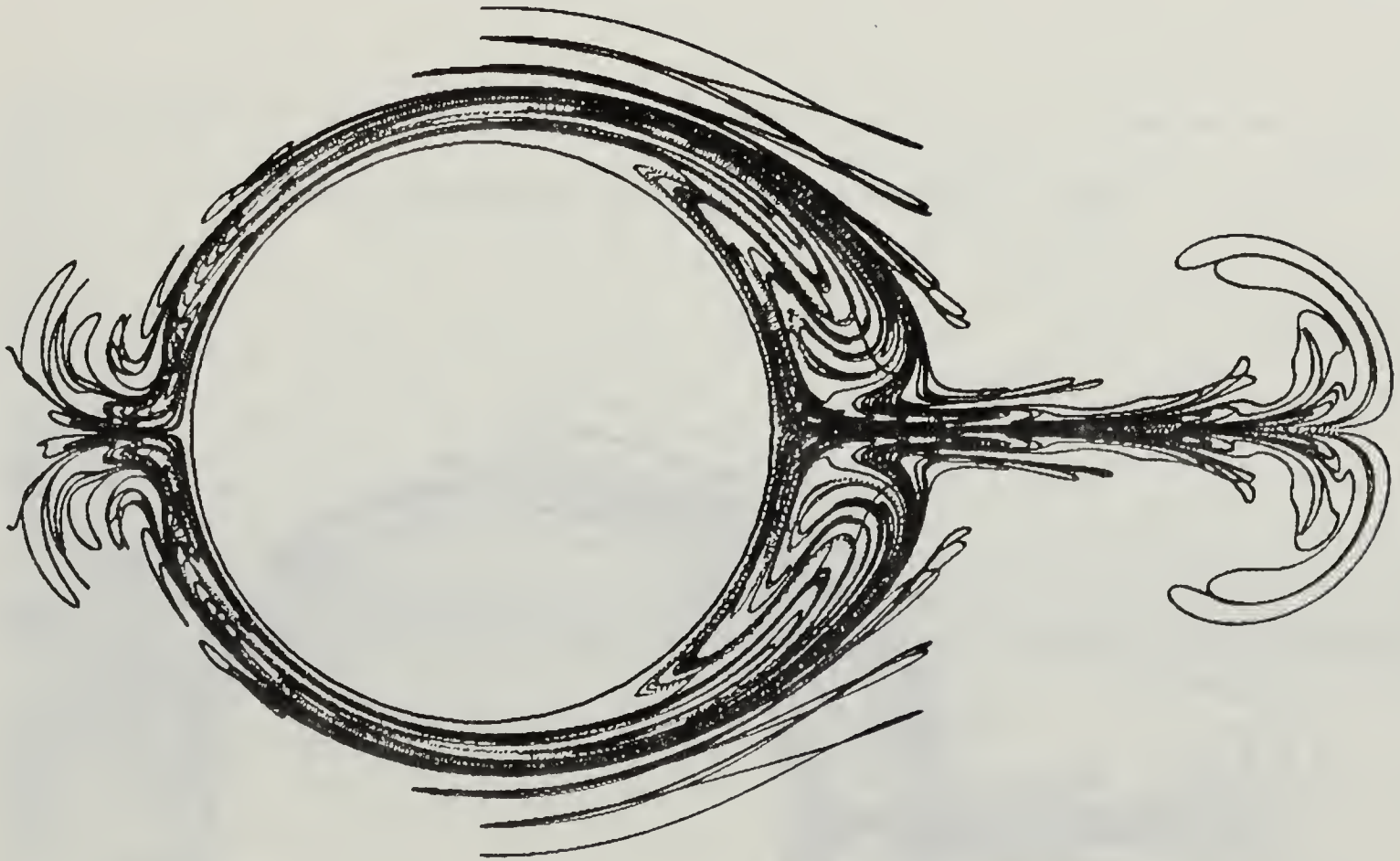

Figure 12. Streaklines, K = 2, Re =400, V_r = 0.0, t/T = 5.0

Figure 13. Streaklines, K = 2, Re =400, V_r = 0.0, t/T = 6.0

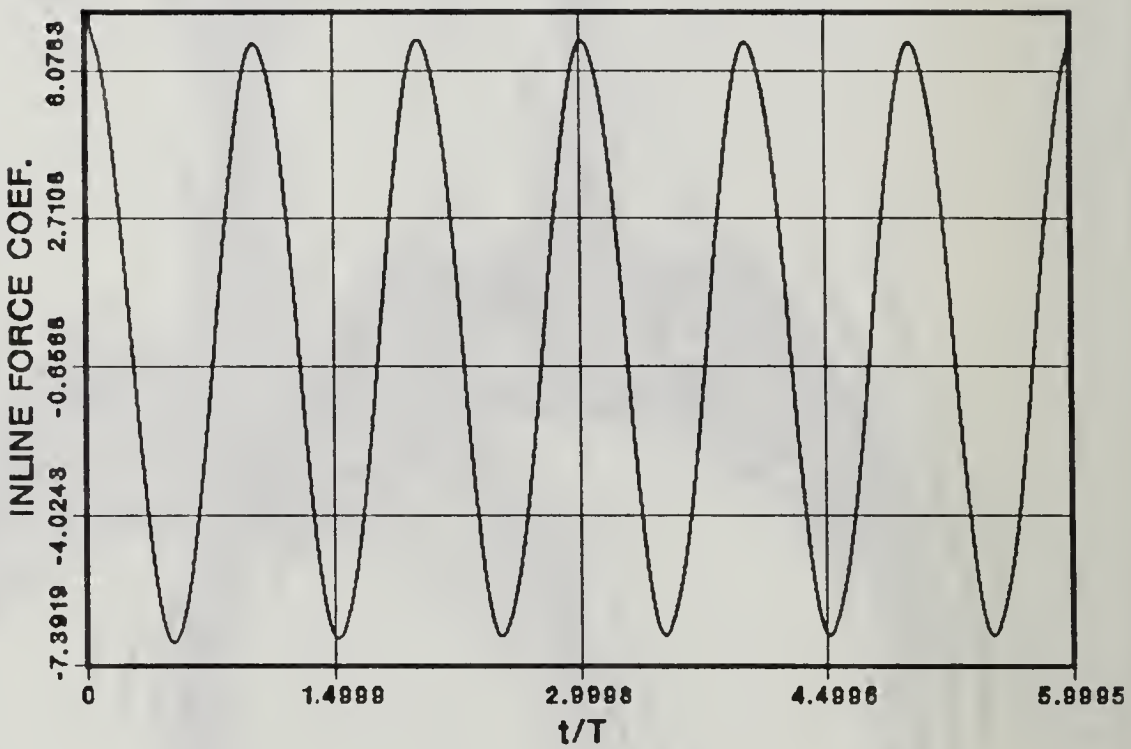

Figure 14. In-Line Force Coefficient, K = 3, Re =600, V_r = 0.0

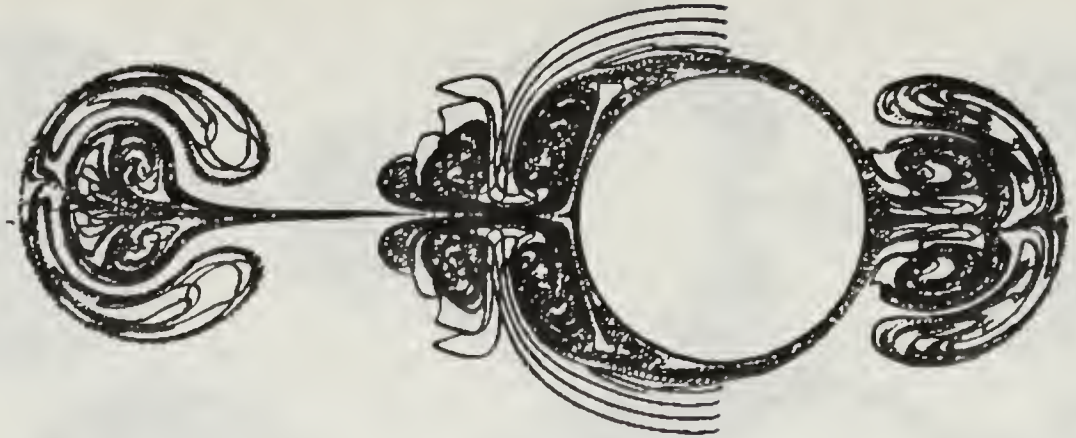

Figure 15. Streaklines, K = 3, Re =600, V_r = 0.0, t/T = 3.0

Figure 16. Streaklines, K = 3, Re =600, V_r = 0.0, t/T = 4.0

Figure 17. Streaklines, K = 3, Re =600, V_r = 0.0, t/T = 4.25

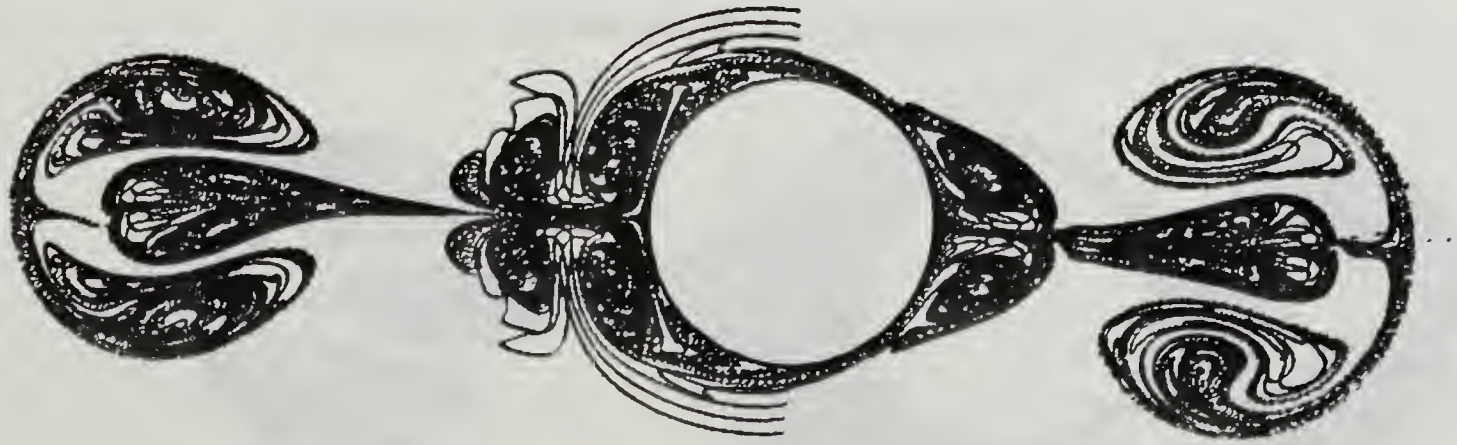

Figure 18. Streaklines, K = 3, Re =600, V_r = 0.0, t/T = 4.50

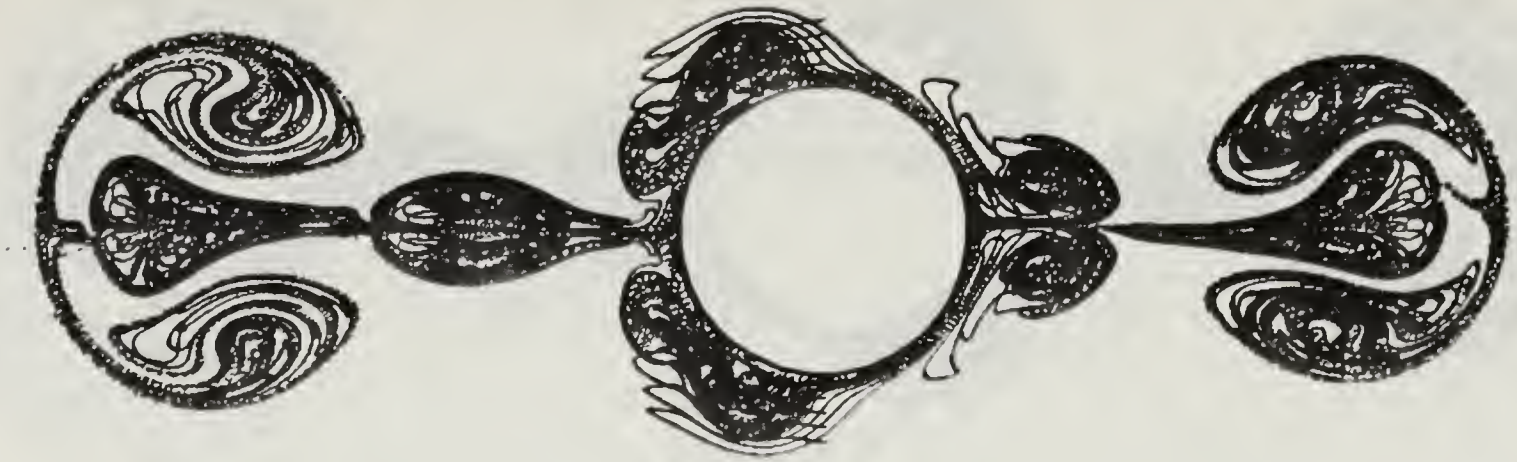

Figure 19. Streaklines, K = 3, Re =600, V_r = 0.0, t/T = 4.75

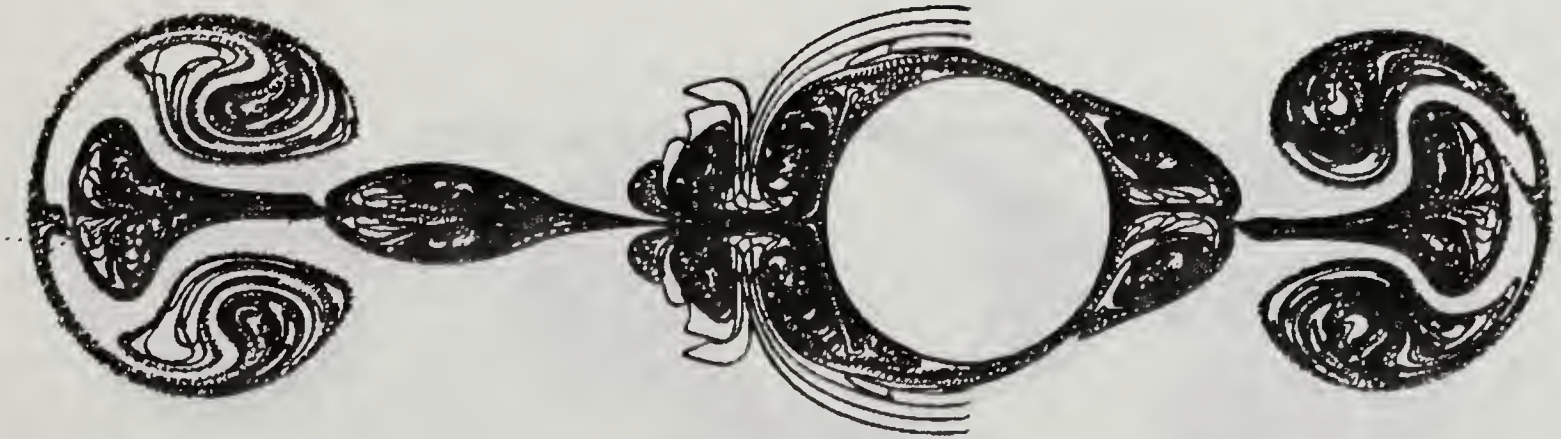

Figure 20. Streaklines, K = 3, Re =600, V_r = 0.0, t/T = 5.0

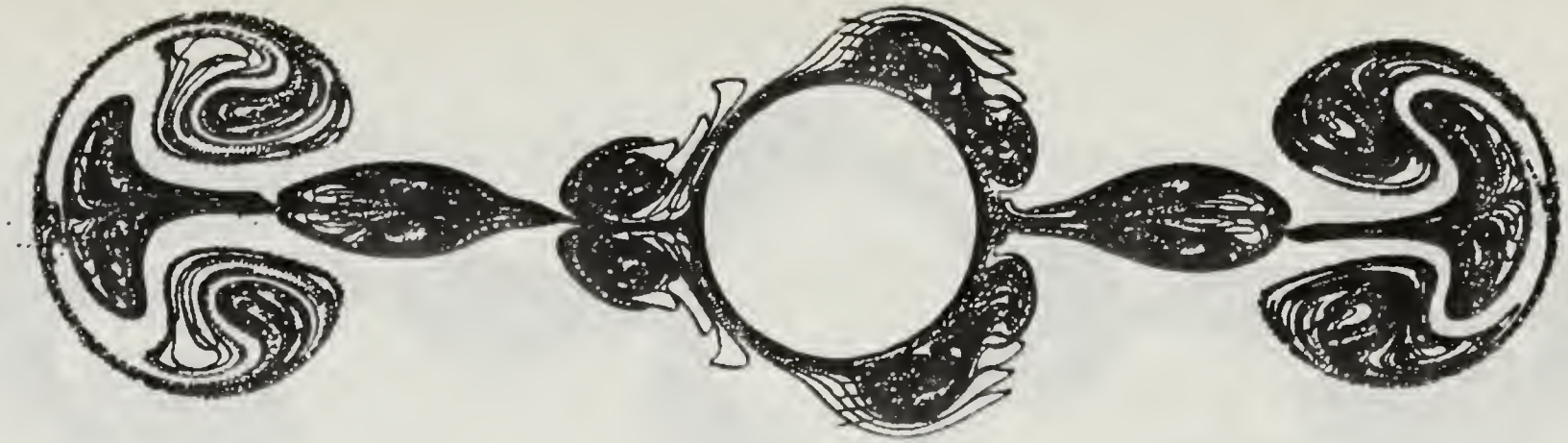

Figure 21. Streaklines, K = 3, Re =600, V_r = 0.0, t/T = 5.25

Figure 22. Streaklines, K = 3, Re =600, V_r = 0.0, t/T = 5.50

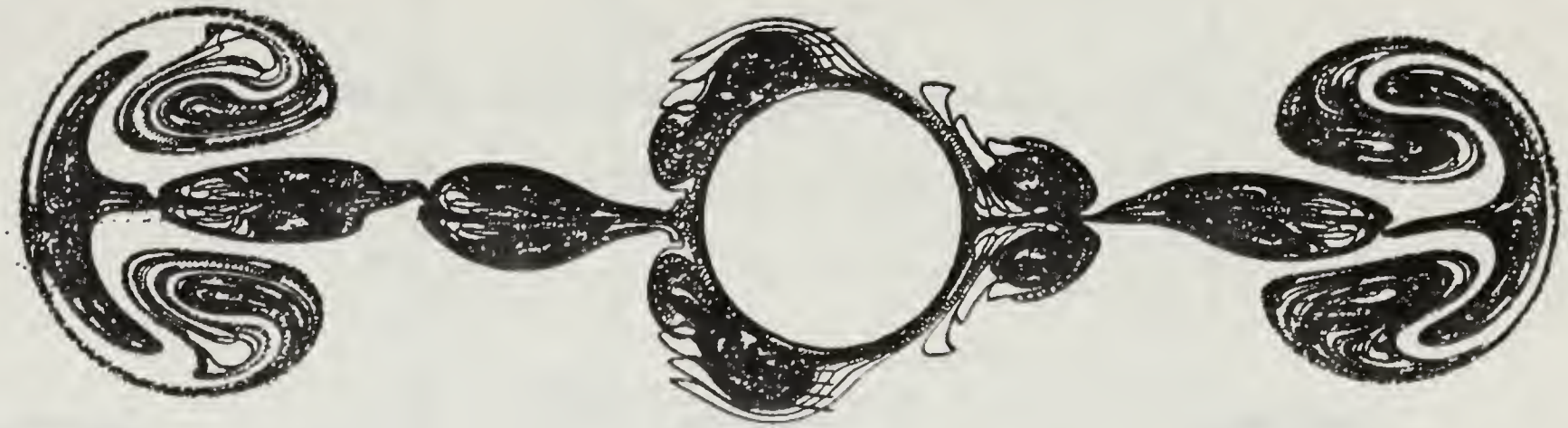

Figure 23. Streaklines, K = 3, Re =600, V_r = 0.0, t/T = 5.75

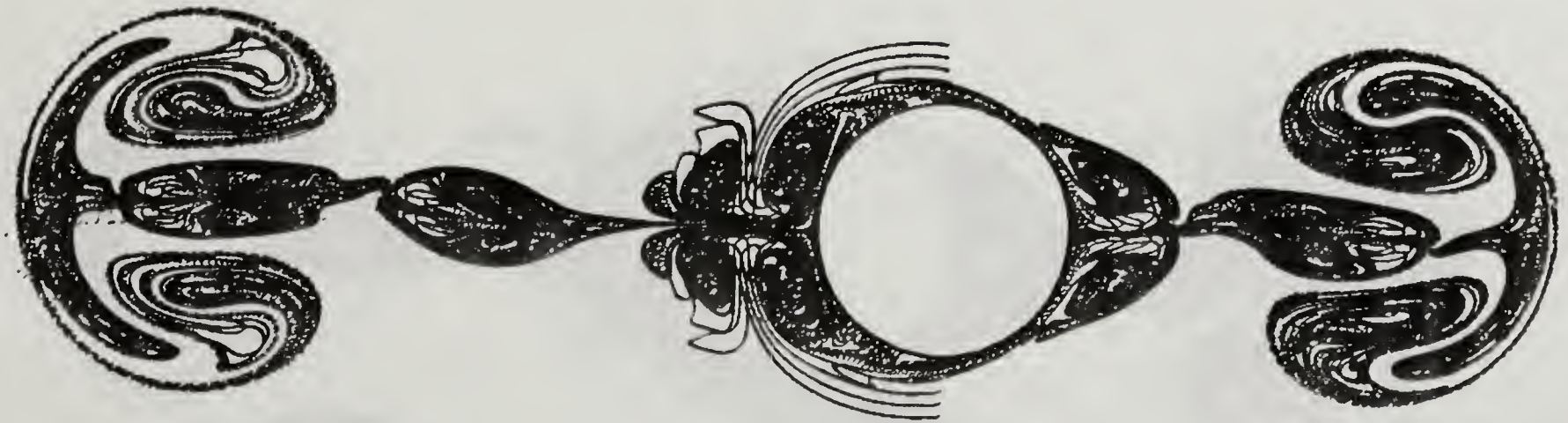

Figure 24. Streaklines, K = 3, Re =600, V_r = 0.0, t/T = 6.0

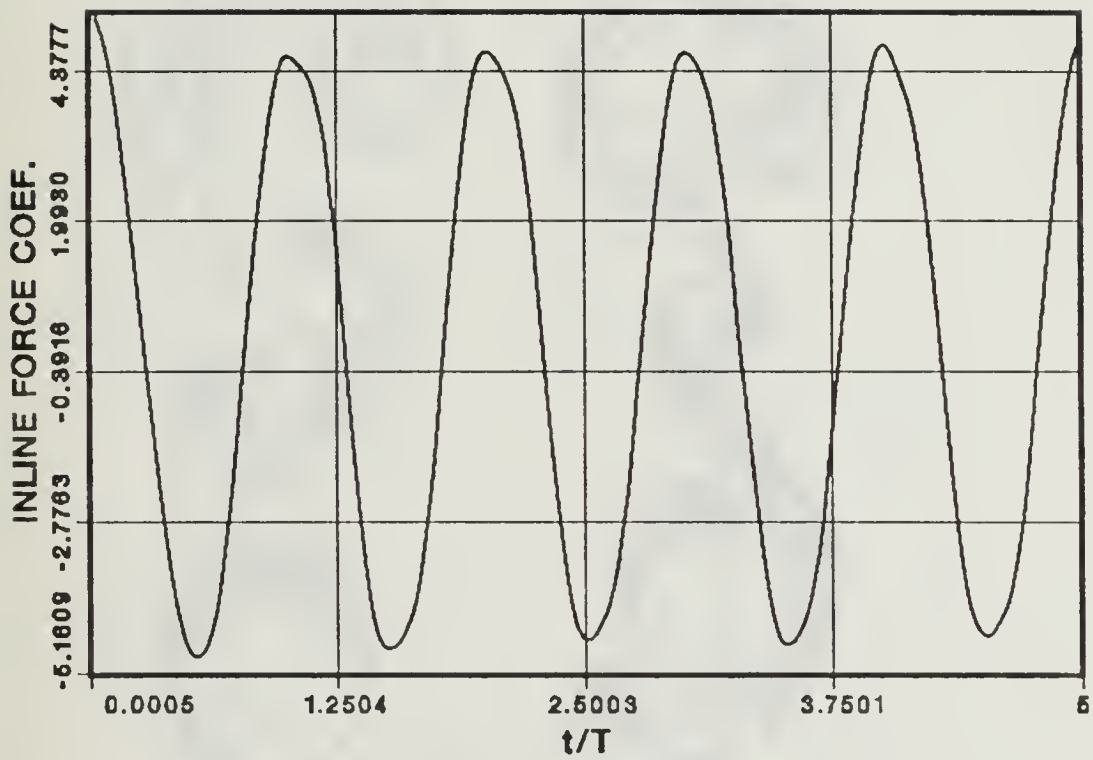

Figure 25. Inline Force Coefficient, K = 4, Re = 800, V_r = 0.0

Figure 26. Streaklines, K = 4, Re =800, V_r = 0.0, t/T = 3.0

Figure 27. Streaklines, K = 4, Re =800, V_r = 0.0, t/T = 4.0

Figure 28. Streaklines, K = 4, Re =800, V_r = 0.0, t/T = 4.25

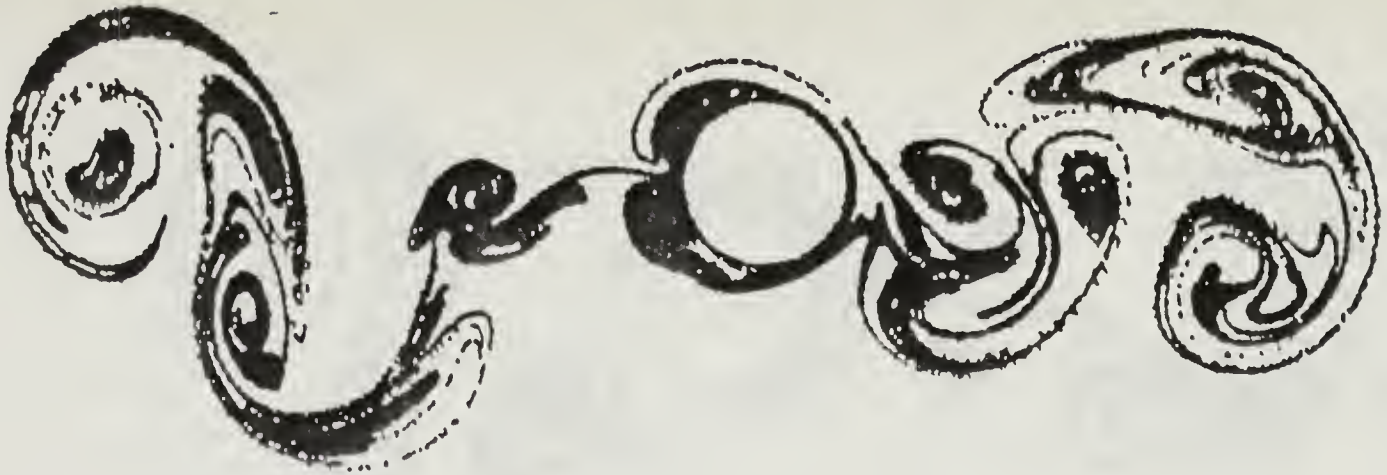

Figure 29. Streaklines, K = 4, Re =800, V_r = 0.0, t/T = 4.50

Figure 30. Streaklines, K = 4, Re =800, V_r = 0.0, t/T = 4.75

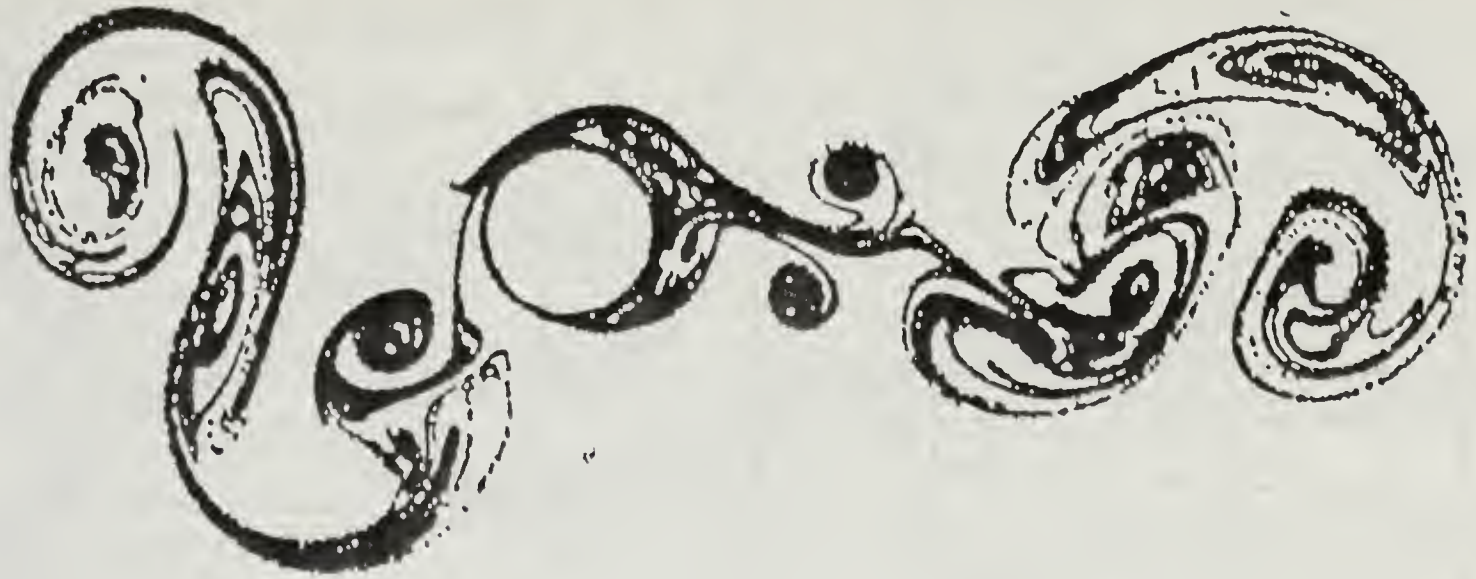

Figure 31. Streaklines, K = 4, Re =800, V_r = 0.0, t/T = 5.0

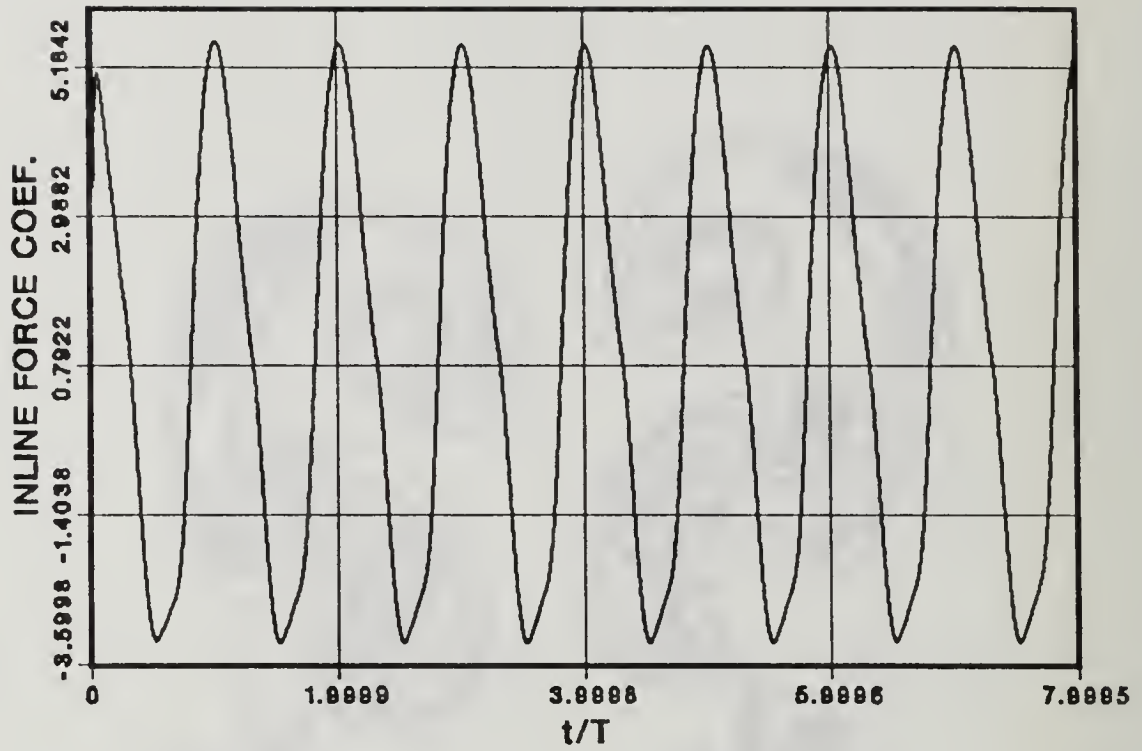

Figure 32. Inline Force Coefficient, K = 4, Re = 800, $V_r = 0.6$

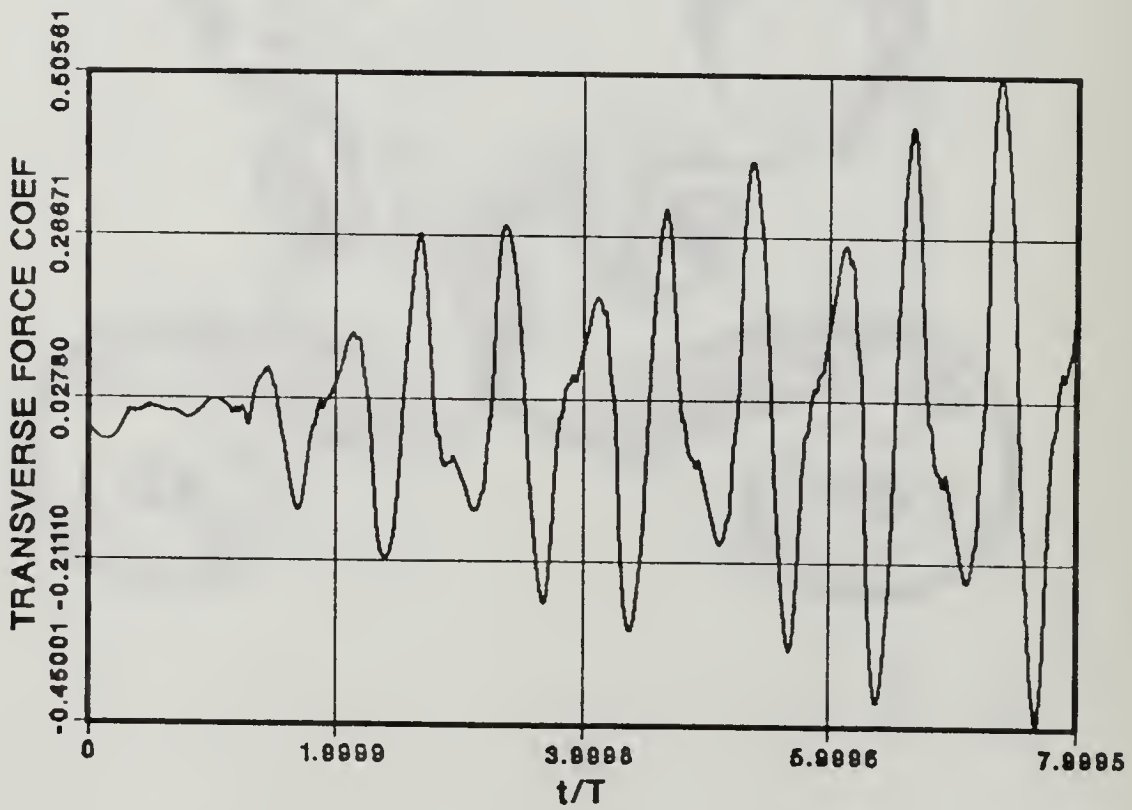

Figure 33. Transverse Force Coefficient, K = 4, Re = 800, $V_r = 0.6$

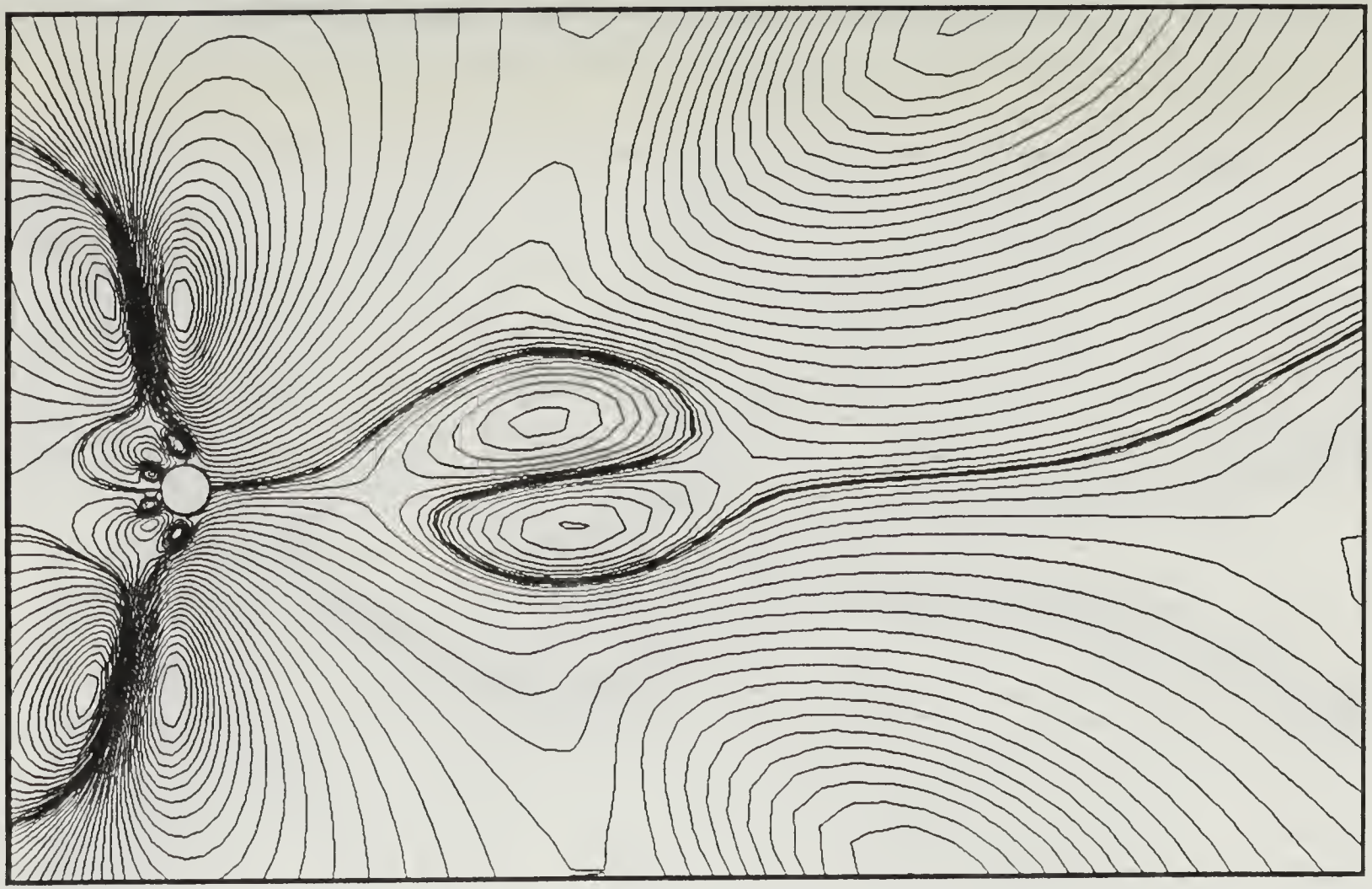

Figure 34. Streamlines, K = 4, Re =800, V_r = 0.6, t/T = 4.0

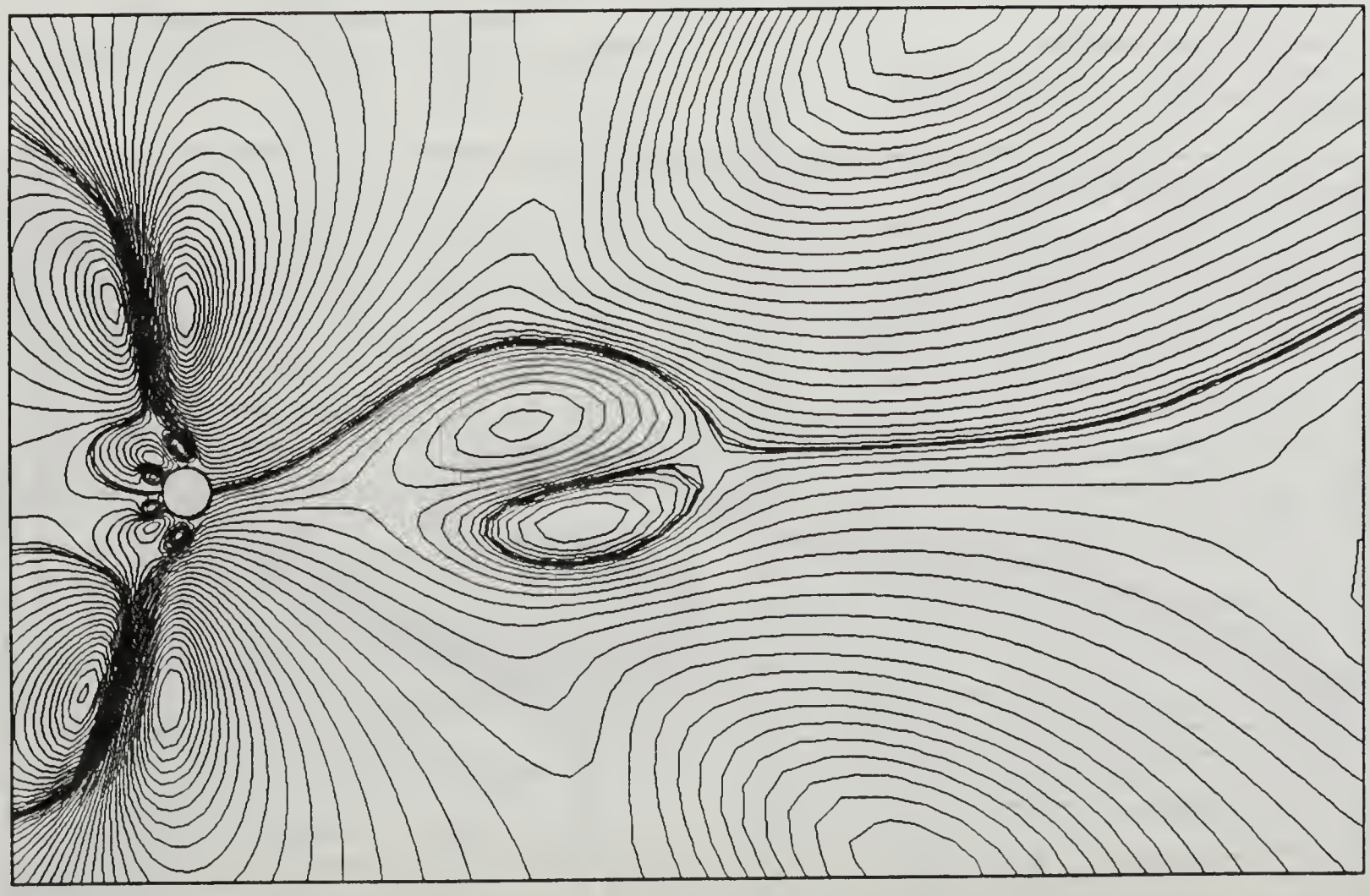

Figure 35. Streamlines, K = 4, Re =800, V_r = 0.6, t/T = 6.0

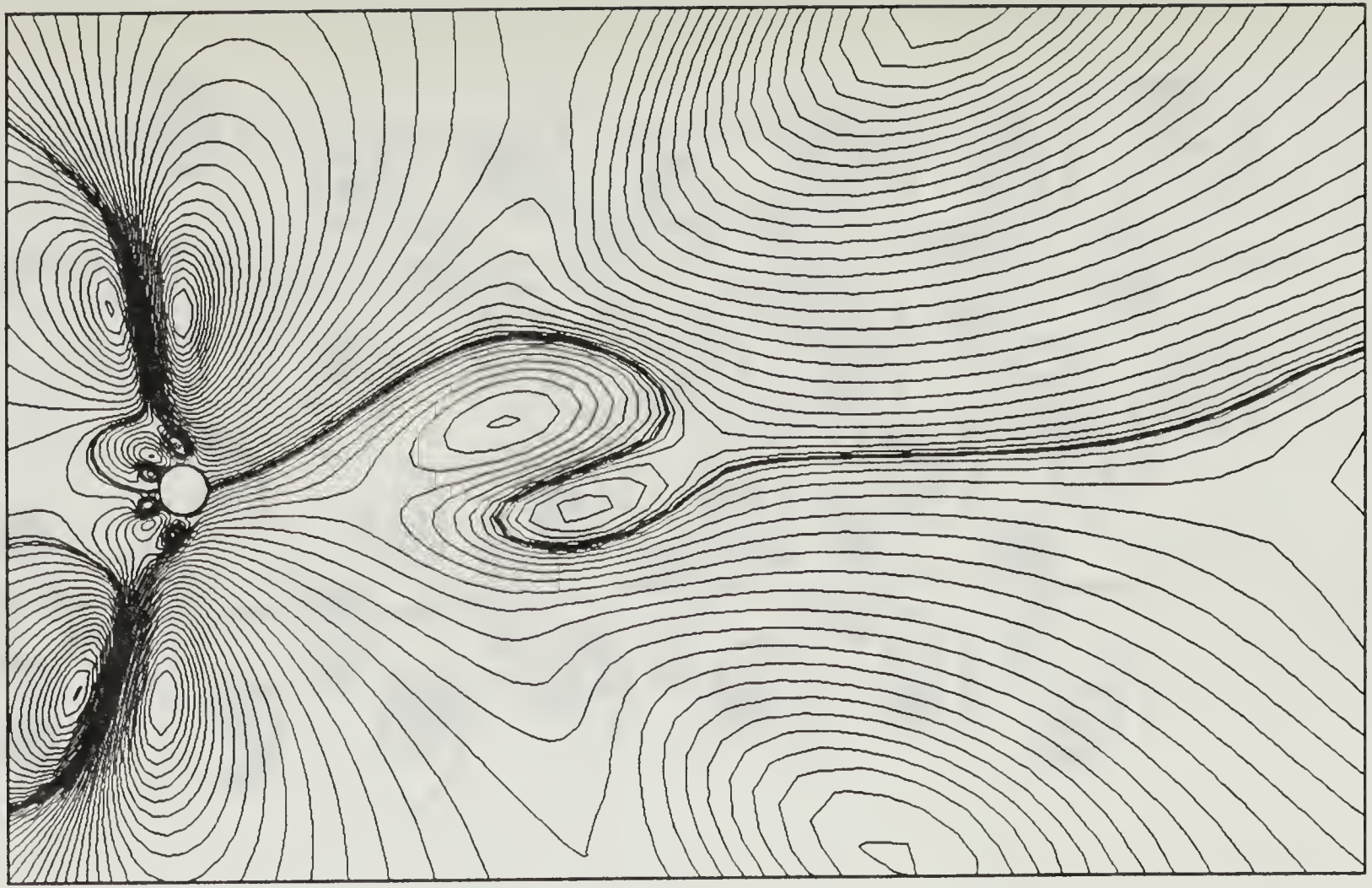

Figure 36. Streamlines, K = 4, Re =800, V_r = 0.6, t/T = 8.0

Figure 37. Streaklines, K = 4, Re =800, $V_r = 0.6$, $t/T = 6.0$

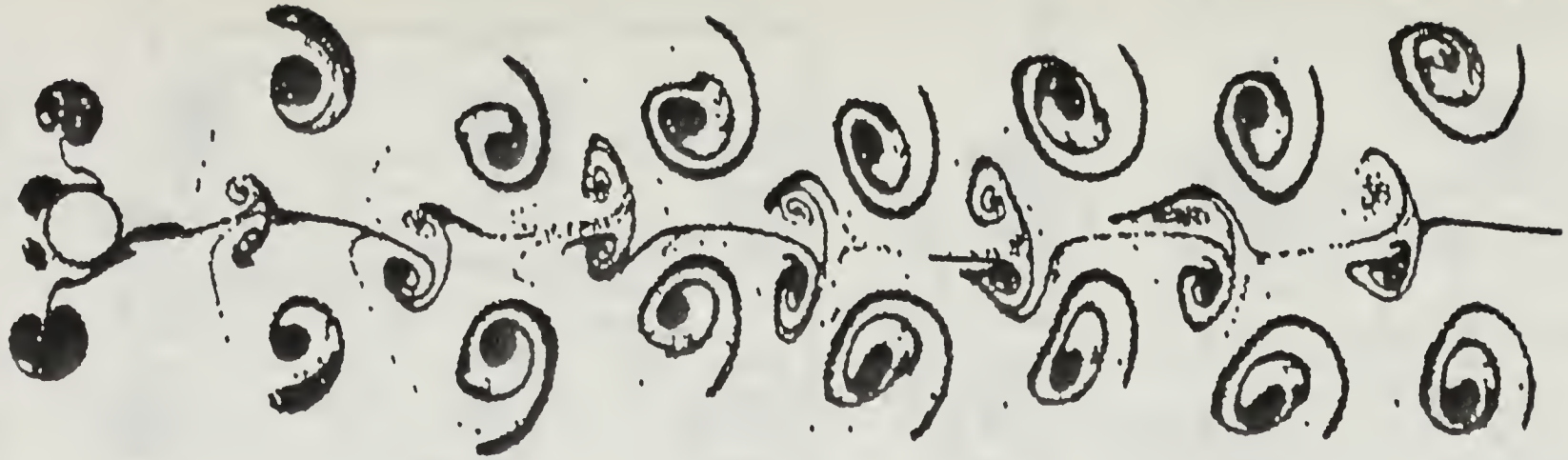

Figure 38. Streaklines, K = 4, Re =800, V_r = 0.6, t/T = 8.0

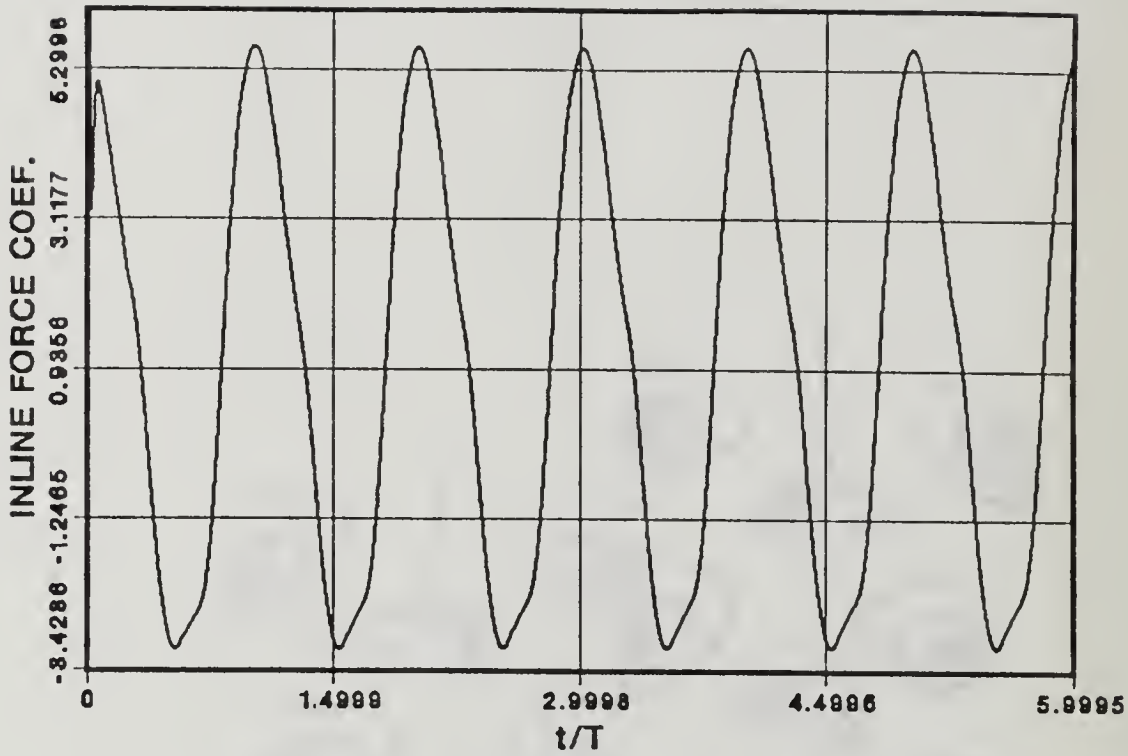

Figure 39. Inline Force Coefficient, K = 4, Re = 800, V_r = 0.65

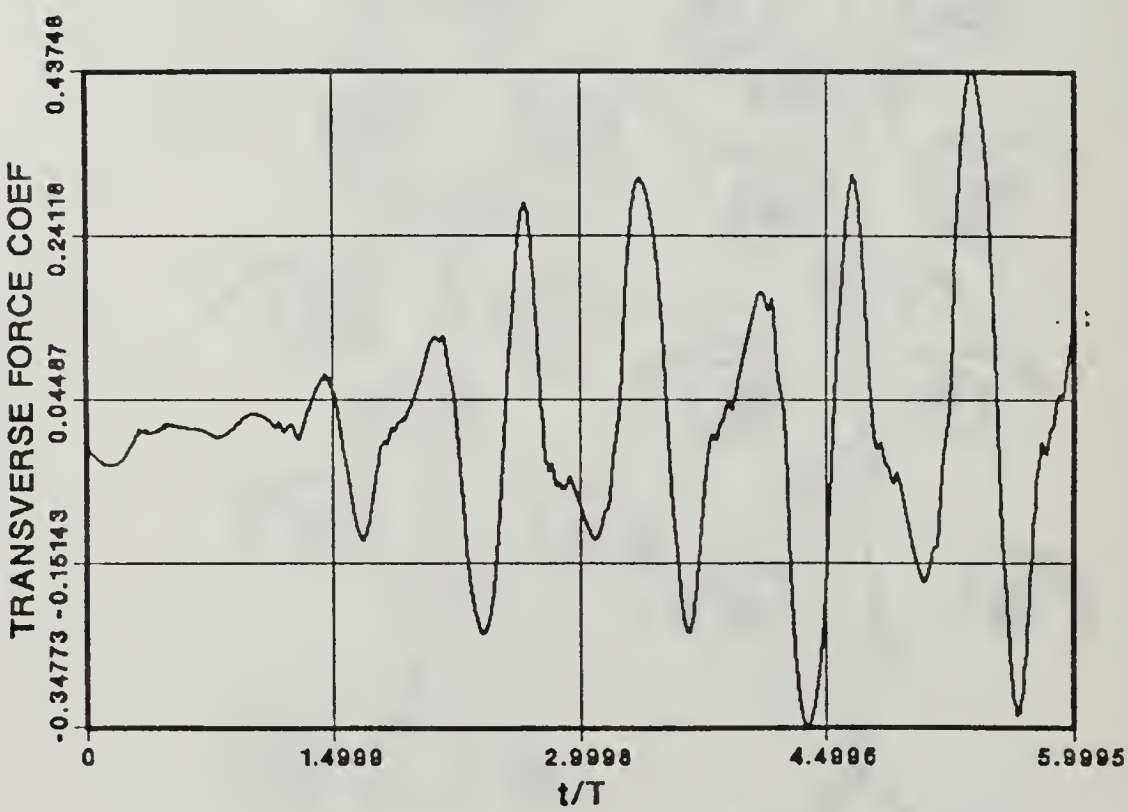

Figure 40. Transverse Force Coefficient, K = 4, Re = 800, V_r = 0.65

Figure 41. Streaklines, K = 4, Re =800, V_r = 0.65, t/T = 6.0

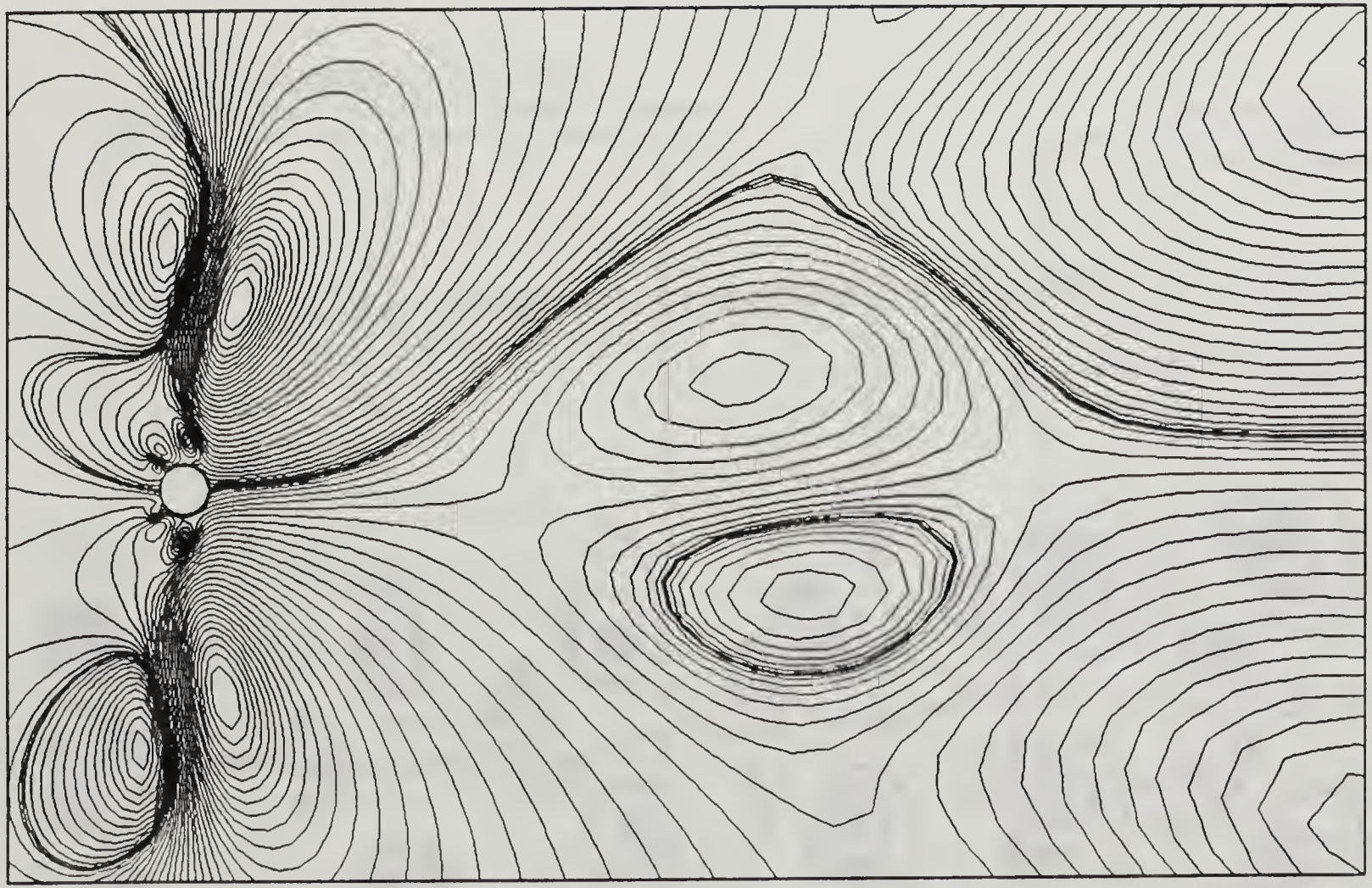

Figure 42. Streamlines, K = 4, Re =800, V_r = 0.7, t/T = 8.0

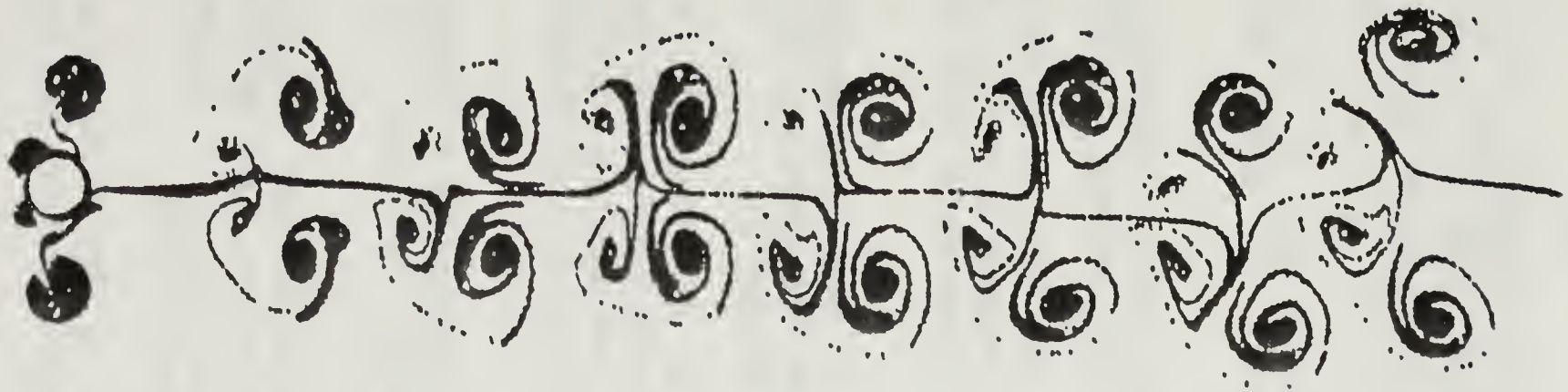

Figure 43. Streaklines, K = 4, Re =800, V_r = 0.7, t/T = 8.0

REFERENCES

1. Baba, N. and Miyata, H., 1987, "Higher-Order Accurate Difference Solutions of Vortex Generation from a Circular Cylinder in an Oscillatory Flow," *Journal of Computational Physics*, Vol. 69, pp. 362-396.

2. Fredrickson, K., 1990, *Numerical Study of Non-impulsively Started Flow Around a Circular Cylinder*, M.S. Thesis, Naval Postgraduate School, Monterey, CA.

3. Justesen, P., 1991, "A Numerical Study of Oscillating Flow Around a Circular Cylinder," *Journal of Fluid Mechanics*, Vol. 222, pp. 157-196.

4 Lecointe, Y., and Piquet, J., 1984, "On the Use of Several Compact Methods for the Study of Unsteady Incompressible Viscous Flow Round a Circular Cylinder," *Computers & Fluids*, Vol. 12, No. 4, pp. 255-280.

5 Moe, G. and Verley, R. L. P., 1980, "Hydrodynamnic Damping of Offshore Structures in Waves and Currents," *Offshore Technology Conference*, Paper OTC 3798, Houston, TX.

6. Murashige, S., Hinatsu, M., and Kinoshita, T., 1989, "Direct Calculations of the Navier-Stokes Equations for Forces Acting on a Cylinder in Oscillatory Flow," In Proceedings of the Eight International Conference on Offshore Mechanics and Arctic Engineering, The Hague, Vol. 2, pp. 411-418.

7. Putzig, C. J., 1990, "Numerical Experiments in Unsteady Flows through the use of Full Navier-Stokes Equations," M.S. Thesis, Naval Postgraduate School, Monterey, CA.

8. Sarpkaya, T. and Butterworth, W., 1991, "Separation Points on a Cylinder in Oscillating Flow," In *Proc. Ninth Intl. Conf. Offshore Mech. and Arctic Engng. Stavanger* (in Press in the *Journal of Offshore Mechanics and Arctic Engineering*, ASME).

9. Sarpkaya, T. and Isaacson, M., 1981, *Mechanics of Wave Forces on Offshore Structures*, Van Nostrand Reinhold, New York, N. Y.

10. Sarpkaya, T. and Storm, M., 1985, "In-line Force on a Cylinder Translating in Oscillating Flow," *Applied Ocean Research*, Vol. 7, No. 4, pp. 188-196.

11. Wang, X., 1989, *A Numerical Study of Unsteady Flows Past A Circular Cylinder*, Ph.D. Dissertation, University of Houston, Houston, Texas.

12. Wang, C. Y., 1968, On High Frequency Oscillating Viscous Flows," *Journal of Fluid Mechanics*, Vol. 32, pp. 55-68.

INITIAL DISTRIBUTION LIST

		No. Copies
1.	Defense Technical Information Center Cameron Station Alexandria, VA 22304-6145	2
2.	Library, Code 52 Naval Postgraduate School Monterey, CA 93943-5002	2
3.	Department Chairman, Code ME Department of Mechanical Engineering Naval Postgraduate School Monterey, CA 93942-5000	2
4.	Professor T. Sarpkaya, Code ME-SL Department of Mechanical Engineering Naval Postgraduate School Monterey, CA 93943-5000	5
5.	LCDR John E. Lotshaw Puget Sound Naval Shipyard Bremerton, WA 98314	3
3.	Curricular Officer, Code 34 Department of Naval Engineering Naval Postgraduate School Monterey, CA 93942-5000	1

DUDLEY KNOX LIBRARY
NAVAL POSTGRADUATE SCHOOL
MONTEREY CA 93943-5101

3 2768 00308752 9